This is the ACCEPTED version of this article. The final, published version of the article can be found at: https://doi.org/10.1016/j.ijthermalsci.2026.111183

Heat transfer characteristics of lead-bismuth eutectic and CO_2-based mixtures in straight-channel printed circuit heat exchangers

Xiaojian Zhang[a], Hao Qiu[a,b,*], Benjamin H. W. Teo[b], Xing Wang[a], Kuihua Han[a], Jianhui Qi[a,*], Christos N. Markides[b]

[a] *School of Energy and Power Engineering, Shandong University, Jinan 250061, China*

[b] *Clean Energy Processes (CEP) Laboratory, Department of Chemical Engineering, Imperial College London, London SW7 2AZ, UK*

[*] *Corresponding authors. E-mail addresses: h.qiu@imperial.ac.uk (H. Qiu); j.qi@sdu.edu.cn (J. Qi)*

Abstract

Lead-cooled fast reactors coupled with supercritical CO_2 Brayton power cycles represent a highly promising energy conversion technology for next generation nuclear power system. The overall thermal performance of these systems can be further enhanced by introducing CO_2-based mixtures, however, investigations on the heat transfer and flow characteristics of lead-bismuth eutectic (LBE) and CO_2-based mixtures in the intermediate heat exchanger between the primary and secondary loops remain scarce. In this work, numerical simulations were conducted to investigate the heat transfer and flow characteristics of LBE and CO_2-based mixtures in straight-channel printed circuit heat exchangers (PCHEs). The performance of CO_2-propane, CO_2-krypton and CO_2-xenon at different mixing mole fractions was compared. The results show that, among the investigated CO_2-based mixtures, the CO_2-propane mixture provides the most favourable heat transfer performance when coupled with LBE. Compared with pure CO_2 under the same operating conditions, the overall heat transfer coefficient of the CO_2-propane/LBE PCHE increases by up to 40%. In addition, the impact of key parameters (e.g., inlet velocity, mass flow rate, inlet temperature, and pressure) on the heat transfer characteristics of CO_2-propane mixtures was analysed. Finally, correlations for the Nusselt number and friction factor were derived using the simulation results, with prediction errors within ±3% for CO_2-propane mixtures with a propane mole fraction in the range 0.05-0.30. This study provides a theoretical foundation for designing and optimizing PCHEs with LBE and CO_2-based mixtures serving as heat transfer media.

Keywords: Brayton cycle; CO_2-based mixtures; Heat transfer; Lead-bismuth eutectic; Printed circuit heat exchanger (PCHE)

Highlights

- We present results from numerical investigations of LBE and CO_2 mixtures in PCHEs
- The effects of key parameters on heat transfer and flow performance are studied
- The performance of CO_2-propane, CO_2-Kr and CO_2-Xe mixtures are compared
- CO_2-propane mixtures provide superior heat transfer performance compared to pure CO_2
- Proposed correlations for CO_2-propane mixtures predict *Nu* and *f* within ±3%

Nomenclature

Abbreviations		*Greek*	
CO_2	carbon dioxide	α	mole fraction of propane
LBE	lead-bismuth eutectic	δ	wall thickness, m
PCHE	printed circuit heat exchanger	λ	thermal conductivity, W/(m·K)
sCO_2	supercritical carbon dioxide	μ	dynamic viscosity, Pa·s
SST	shear stress transport	μ_t	turbulent viscosity, Pa·s
UDF	user defined function	ρ	density, kg/m^3
		ω	turbulent dissipation rate, m^2/s^2
Symbols			
c_p	specific heat capacity at constant pressure, J/(kg·K)	*Subscripts*	
		avg	average
D	diameter, m	c	cold side
f	friction factor	eff	effective
h	convective heat transfer coefficient, W/(m^2·K)	h	hot side
		hyd	hydraulic
k	turbulent kinetic energy, m^2/s^2	in	inlet condition
L	characteristic length, m	mix	CO_2-based mixtures
Nu	Nusselt number	out	outlet condition
Pe	Peclet number	s	solid
Pr	Prandtl number		
Pr_t	turbulent Prandtl number		
q	heat flux, W/m^2		
Re	Reynolds number		
R_{pre}	predictive results using correlations		
R_{sim}	simulation results		
T	temperature, K or °C		
U	overall heat transfer coefficient		
v	velocity, m/s		
ΔP	pressure drop, Pa		

1. Introduction

As the global energy system undergoes an accelerated transition to low-carbon strategies, nuclear energy has become a crucial technology for achieving carbon neutrality, owing to its zero carbon emissions, high energy density, and excellent load-following capability in power grids [1]. Among various reactor types, the lead-bismuth fast reactor employs liquid lead-bismuth eutectic (LBE) as the coolant. It exhibits inherent safety advantages such as excellent neutron economy, operation at near-atmospheric pressure, and a high boiling point [2]. Moreover, the high core outlet temperature of LBE (up to 550-800 °C) provides favourable conditions for efficient energy conversion in advanced nuclear systems [3].

The supercritical carbon dioxide (sCO_2) Brayton cycle is recognized as a promising energy conversion technology for next-generation energy systems. Thanks to its high thermal efficiency, compactness and power density, and lower turbine operating temperatures [4,5], it has received significant attention in the context of waste-heat recovery and conversion [6–8], power generation from solar [9–11] and geothermal [12,13] heat sources, as well as for hybrid energy-source conversion [14,15], or as part of energy storage technologies [16,17].

Compared to conventional Rankine cycles and gas turbines, the sCO_2 cycle achieves high thermal efficiency in the temperature range of 450-650 ℃ [18], which is closely corresponds to the operating temperatures of advanced nuclear reactors [19,20]. Previous studies have shown that when the lead-bismuth fast reactor system is coupled with the sCO_2 cycle, the thermal efficiency of this system can exceed 50% [21,22]. As the core component of this energy conversion system, the intermediate heat exchangers not only facilitate heat transfer but also play a critical role in radioactive isolation [23]. The printed circuit heat exchanger (PCHE) is characterized by its compact microchannel structure, high thermal efficiency, resistance to high temperatures and pressures, and suitability for natural circulation [24]. Owing to these advantages, it has been widely considered a promising component for heat exchange applications in various reactor designs [25–27].

Nevertheless, the critical temperature and pressure of pure CO_2 (T = 304.1 K, P = 7.38 MPa) [5] limit its cycle performance under high ambient temperatures or fluctuating heat source conditions. Based on Carnot cycle theory, reduced critical temperature and pressure increases both the temperature range available to the cycle and the attainable pressure ratios, thereby improving the cycle efficiency [28]. Small amounts of propane, krypton, or xenon are often introduced to form CO_2-based mixtures. In this way, the critical properties of the CO_2-based mixtures can be modified depending on the type and

fraction of the added gas [29,30]. Typically, the addition of propane elevates the critical temperature, while noble gases such as krypton and xenon reduce the critical temperature. Invernizzi et al. [31] performed a comparative analysis of different CO_2-based binary mixtures, and their efficiency exceeds that of the pure CO_2 cycle. Guo et al. [32] evaluated the viability of employing xenon and found that the system efficiency is improved by 1.4-1.6%. Liu et al. [33] developed a thermodynamic and heat exchanger heat transfer model using Aspen Plus. Under high-temperature cooling conditions, the cycle with CO_2-based mixtures exhibited superior thermal efficiency. Among the investigated mixtures, CO_2-propane exhibited the best performance in heat exchanger. Ma et al. [34] conducted a thermal-economic analysis of the CO_2-based mixtures in the Brayton cycle. The results indicated that the CO_2-Kr cycle offers comprehensive advantages in efficiency improvement and cost control, whereas the CO_2-Xe cycle demonstrates a notable increase in efficiency and is more suitable for high-temperature and high-pressure conditions. These findings indicate that the incorporation of CO_2-based mixtures is a crucial approach for the enhancement of the Brayton cycle's efficiency.

Numerous studies have been conducted previously on the heat transfer and flow characteristics of sCO_2 flows, which has attracted significant attention due to the complex thermohydraulic behaviour of these flows. For example, the thermal and hydraulic characteristics of upward and downward supercritical CO_2 flows in vertical tubes were investigated by Guo et al. [35] in heated and Guo et al. [36] in cooled conditions, and Sun et al. [37] developed a new heat transfer prediction model based on artificial neural networks (ANN) for the case of heated upwards flows. The specific case of sCO_2 and LBE flows in PCHEs relevant to lead-based reactors has also received attention; e.g., Liu et al. [38] compared various PCHE structures, including straight, zigzag and combined channels. The combined channel was found to achieve an optimum performance between heat transfer and flow resistance. Zhou et al. [39] developed an analysis of a turbulent Prandtl number (Pr_t) model for LBE and verified that, under high buoyancy conditions in the near-critical region, heat transfer within the cold channel emerges as the dominant transport mechanism. Xu et al. [40] simulated the heat transfer and flow characteristics of LBE and sCO_2 in PCHE. The study found that the inlet flow rate, temperature difference, pressure and geometric parameters have significant impact on the overall heat transfer coefficient. Furthermore, Fu et al. [41] conducted targeted optimization of the PCHE and provided correlations in the optimal "rectangular-to-two"

channel. However, most of these studies focus on LBE and pure CO_2 as working fluids, while research on the coupling characteristics of LBE and mixed fluids in PCHEs remains scarce.

In recent years, some studies have focused on the application potential of mixed working fluids in microchannel heat exchangers. Kim et al. [42] provided thermophysical data for helium-CO_2 mixtures and proposed empirical correlations for the friction number *f* and Nusselt number *Nu* applicable to PCHEs. Zhang et al. [28] simulated CO_2-H_2S and CO_2-propane mixtures flowing through finned-surface channels under cooling conditions, identifying buoyancy effects as the dominant mechanism for heat transfer enhancement. Yin et al. [43,44] found that CO_2-propane mixtures achieve higher fluid temperatures and lower pressure drops in the corrugated channel PCHE, with the *Nu* in cold and hot sides increasing by approximately 3% and 17%, respectively. Additionally, a critical heat flux criterion and a *Nu* correlation for supercritical CO_2-propane mixtures were proposed. Yan et al. [45] studied the CO_2-Xe mixtures in a horizontal circular tube and assessed the impact of xenon mass fraction, heat flux, mass flow rate and buoyancy effects. Ma et al. [46] investigated CO_2-Kr mixtures and proposed a heat transfer correlation with a prediction accuracy within ±5%. Zhou et al. [47,48] simulated CO_2 mixed with butane, propane and xenon in PCHEs employing molten salts as hot fluid, respectively. It is found that butane reduces the cold-side pressure-drop significantly.

As mentioned earlier, existing studies have shown that CO_2-based mixtures hold significant application potential in the Brayton cycle and further exhibit excellent heat transfer characteristics when applied in PCHEs. However, current research remains primarily focused on single-fluid conditions, with a lack of studies on the coupling characteristics of LBE and CO_2-based mixtures in PCHEs which is identified as a research gap of interest.

In this work, numerical simulations on a straight-channel PCHE are conducted, in which LBE is used as the hot-side fluid and CO_2-based binary mixtures (CO_2-propane, CO_2-krypton, and CO_2-xenon) are used as the cold-side fluids. Subsequently, the basic performance of these mixtures is compared. In addition, the effects of key operating conditions on the flow and heat transfer characteristics of PCHE are analysed. Lastly, correlations of *Nu* and *f* are determined for practical use in the design of relevant PCHEs. This work clarifies the heat transfer mechanisms between LBE and CO_2-based mixtures in PCHEs, thereby providing theoretical support for the design and optimization in next-generation nuclear and other systems.

2. Mathematical model and numerical methods

2.1. Physical model and boundary conditions

To improve computational efficiency, a representative straight channel unit was adopted as the physical model, leveraging the geometric symmetry and periodicity of PCHEs. As shown in Figure 1, the computational domain consists of hot and cold channels. The upper channel carries liquid LBE as the hot fluid, while the lower channel carries CO_2-based mixtures as the cold fluid. The two fluids flow in a counter-current arrangement. The height and width of PCHE unit are 3.2 mm and 2.5 mm, respectively. The hot-side LBE channel was specified as a velocity inlet to represent the pump-controlled liquid-metal flow in the primary loop, whereas the cold-side CO_2-based mixture channel was specified as a mass-flow inlet to ensure a consistent inlet mass flow rate for different CO_2-based mixture cases.

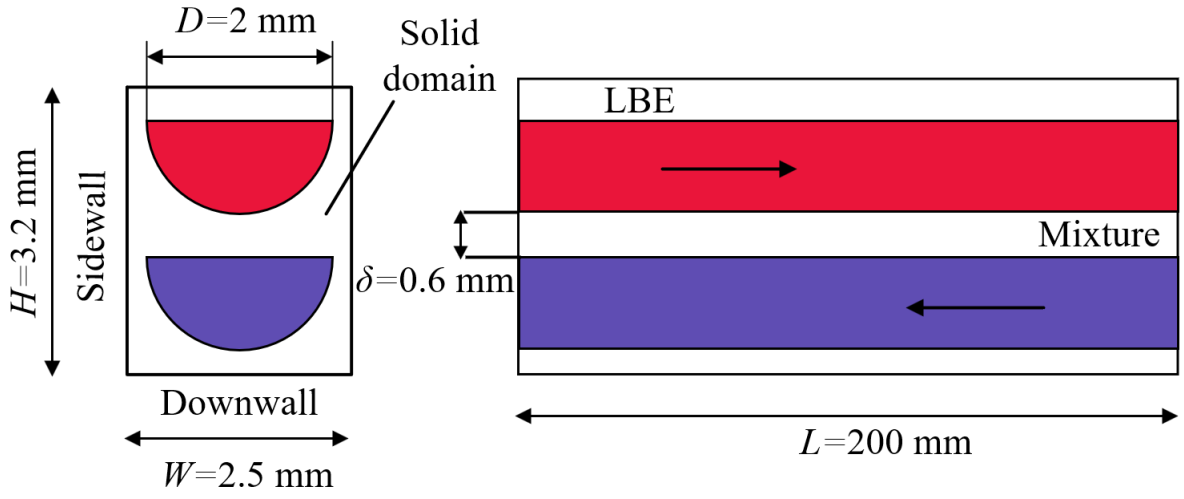

Figure 1. Geometric model of a PCHE unit showing the hot and cold flow path structure and key geometric parameters.

2.2. Governing equations and calculation formulas

In this work, numerical analysis of the PCHE was carried out using ANSYS Fluent 2023. The simulations are conducted with the following assumptions: (i) the fluid flows in steady state condition; (ii) negligible heat transfer between the computational domain and the external environment; and (iii) no internal heat sources. To consider the turbulent effects, the shear stress transport (SST) k-ω model is employed, owing to the demonstrated accuracy in resolving near-wall flow and heat transfer, together with its reduced sensitivity to inlet turbulence parameters [33-35]. The steady-state flow and heat exchange processes can be described by the following governing equations, such as the continuity, momentum and energy equations:

$$\frac{\partial}{\partial x_i}\left(\rho u_i\right)=0, \tag{1}$$

$$\frac{\partial}{\partial x_j}\left(\rho u_i u_j\right)=\frac{\partial}{\partial x_j}\left[\left(\mu_t+\mu\right)\left(\frac{\partial u_i}{\partial x_j}+\frac{\partial u_j}{\partial x_i}-\frac{2}{3}\frac{\partial u_k}{\partial x_k}\right)\right]-\frac{\partial p}{\partial x_i}+\rho g_i, \tag{2}$$

$$\frac{\partial}{\partial x_i}\left(\rho u_i c_p T\right)=\frac{\partial}{\partial x_i}\left(\lambda\frac{\partial T}{\partial x_i}\right)+\dot{\Phi}. \tag{3}$$

where ρ is the density, u the velocity, μ and μ_t the molecular and turbulent viscosities, λ the thermal conductivity, T the temperature, and $\dot{\Phi}$ denotes the viscous dissipation term. In the simulations, convergence is achieved when the residual of the continuity equation is below 1×10^{-6}, and the residuals of the other governing equations are below 1×10^{-8}.

In subsequent calculations, the convective heat transfer coefficient h is defined by:

$$h=\frac{q}{T_\mathrm{b}-T_\mathrm{w}}. \tag{4}$$

The dimensionless Nusselt number Nu is expressed by:

$$Nu=\frac{hD_{hyd}}{\lambda}. \tag{5}$$

The characteristic length D_hyd (hydraulic diameter) is defined by:

$$D_\mathrm{hyd}=\frac{4A}{l}=\frac{\pi D}{\left(\pi+2\right)}. \tag{6}$$

The dimensionless Peclet number, Pe, reflects the relative importance of convection and diffusion, is defined by:

$$Pe=\frac{v\rho c_p D_{hyd}}{\lambda}. \tag{7}$$

The Darcy friction factor f is given by:

$$f=\frac{\Delta p}{\frac{1}{2}\rho v^2\frac{L}{D_{hyd}}}. \tag{8}$$

The overall heat transfer coefficient U of PCHE is expressed by:

$$U = \frac{1}{\frac{1}{h_{\mathrm{LBE}}} + \frac{\delta}{\lambda_{\mathrm{s}}} + \frac{1}{h_{\mathrm{mix}}}}, \tag{9}$$

where h_{LBE} and h_{mix} denote the convective heat transfer coefficients in the hot and cold fluids, respectively, λ_{s} is the thermal conductivity of the solid, and δ is the wall thickness.

3. Validation of numerical methods

3.1. LBE thermophysical properties and validation of turbulent Prandtl number

LBE is a binary alloy composed of 44.5 wt.% lead and 55.5 wt.% bismuth. The thermophysical properties of this mixture were derived by using correlations provided in the OECD/NEA handbook [52]. The correlations for density, specific heat at constant pressure, thermal conductivity, and viscosity are summarized in Table 1.

Table 1. Thermophysical properties of LBE (400-1100 K) [52].

Properties	Correlations	Units
Density, ρ	$\rho = 11065 - 1.293T$	kg/m^3
Specific heat, c_p	$c_p = 164.8 - 3.94\times10^{-2}T + 1.25\times10^{-5}T^2 - 4.56\times10^{5}T^{-2}$	J/(kg·K)
Thermal conductivity, λ	$\lambda = 3.284 + 1.617\times10^{-2}T - 2.305\times10^{-6}T^2$	W/(m·K)
Viscosity, μ	$\mu = 4.94\times10^{-4}\exp\left(\frac{754.1}{T}\right)$	Pa·s

To evaluate the applicability of various turbulence transport models (i.e., turbulent Prandtl number models) in liquid metal simulations, a circular tube model identical in Johnson's experiment [53] was established for numerical calculations (see Figure S1). Six meshes with different cell counts were generated using ICEM to conduct a grid independence test. As shown in Figure 2(a), mesh refinement above 3,389,239 has little influence on the results. Therefore, a mesh with 3,389,239 cells was selected for subsequent simulations to achieve a balance between computational accuracy and efficiency.

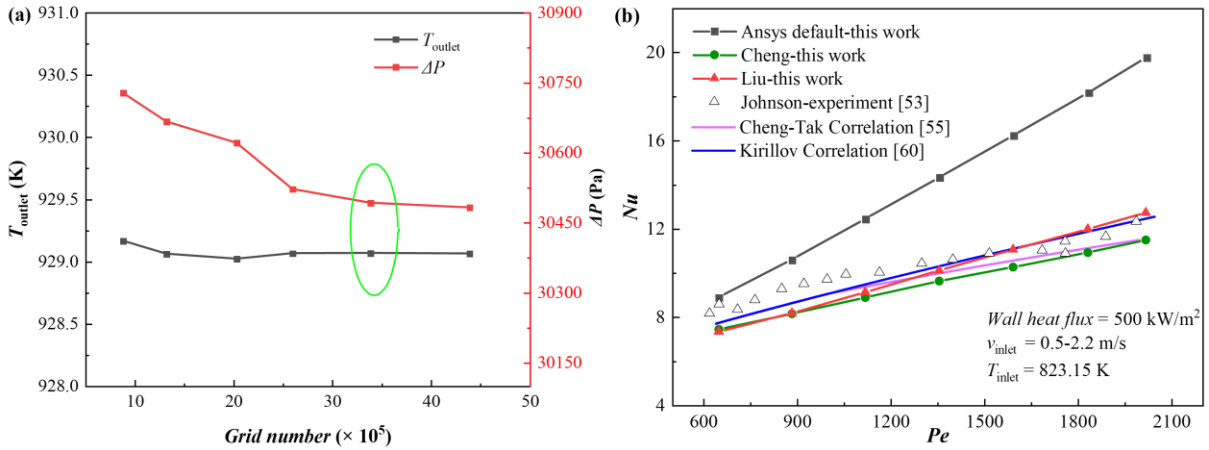

Figure 2. (a) Grid independence verification for the circular tube, and (b) Pr_t model validation for heat transfer.

In this study, three turbulent Prandtl number Pr_t models were used for simulations: the models proposed by Liu et al. [54], Cheng and Tak [55] and the default model in Fluent [56]. All models were implemented and solved through user-defined functions (UDFs). The results are shown in Figure 2(b). As shown, the default $Pr_t = 0.85$ model in Fluent fails to describe turbulent heat transfer in liquid metals accurately, whereas the model by Liu et al. (Eqs. (10) and (11)) exhibits good agreement with both existing correlations [54] and experimental data [53], confirming its suitability for subsequent liquid-metal turbulent heat transfer simulations:

$$Pr_t = 0.85 + \frac{3.5}{Pe_t} \tag{10}$$

$$Pe_t = \frac{\mu_t}{\mu} Pr \tag{11}$$

3.2. Validation of sCO_2 heat transfer in PCHEs

The balance between numerical accuracy and computational efficiency of the simulation is verified based on the study of Meshram et al. [57] shown in Figure 3(a). Six mesh numbers were generated to evaluate the influence of mesh resolution on the simulation results. In Figure 3(b), the comparison of hot-side outlet temperature and pressure drop shows negligible changes with further mesh refinement beyond 3,436,979 cells. Consequently, a mesh containing 3,436,979 cells was employed for subsequent simulations to ensure numerical accuracy while maintaining computational efficiency.

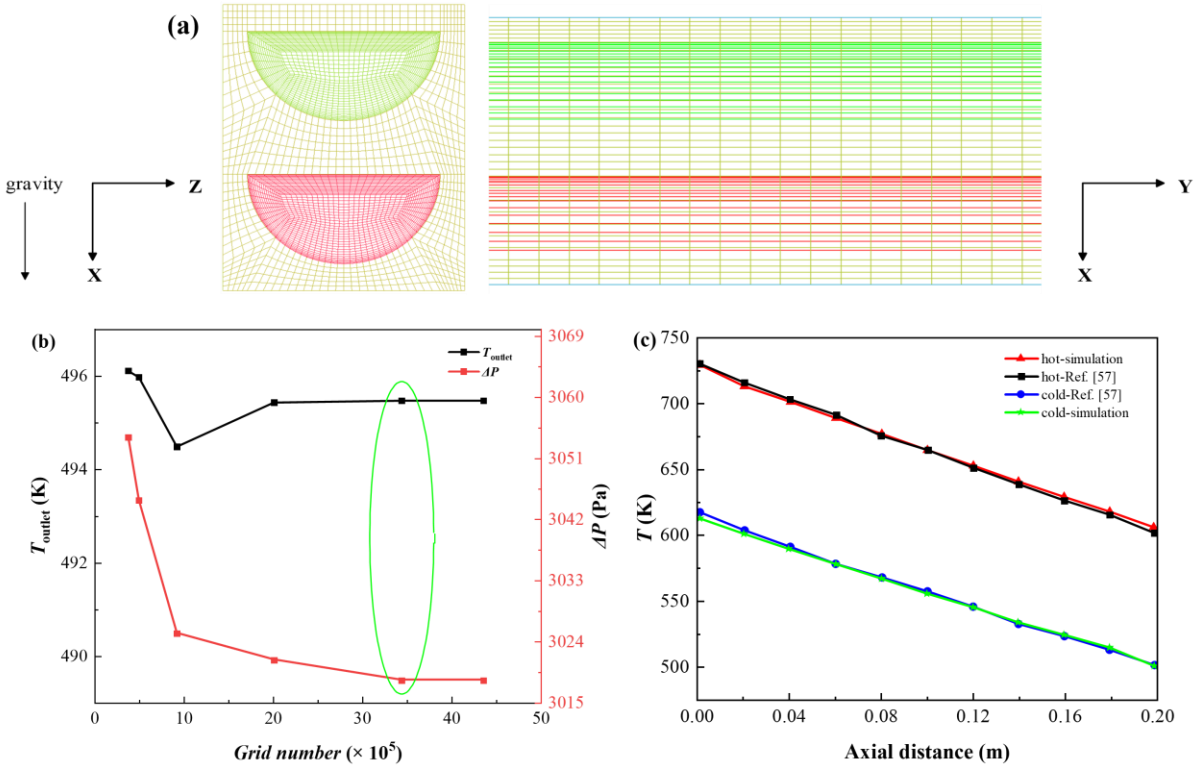

Figure 3. (a) Mesh division of the PCHE unit, (b) mesh number independence verification for the PCHE, and (c) numerical model validation.

To validate the numerical model adopted in this study, the simulation values were compared to the results of Meshram et al. [57] under identical inlet and outlet boundary conditions, as shown in Figure 3(c). The predicted temperature distribution exhibits a trend consistent with the literature, demonstrating that the present method can reliably capture the key parameters of sCO_2 heat transfer in PCHEs.

To further validate the numerical model, the present simulation results were compared with the experimental data reported in Ref. [58]. The same geometric configuration and operating conditions were adopted. Figure 4 compares the predicted heat transfer rate Q_h and pressure drop ΔP_h on hot channel with the experimental results. Good agreement is achieved, with deviations within 5.67% under the conditions of case1 and 3.53% under the conditions of case2. These results further demonstrate the reliability of the present numerical model for predicting thermal-hydraulic characteristics in PCHEs.

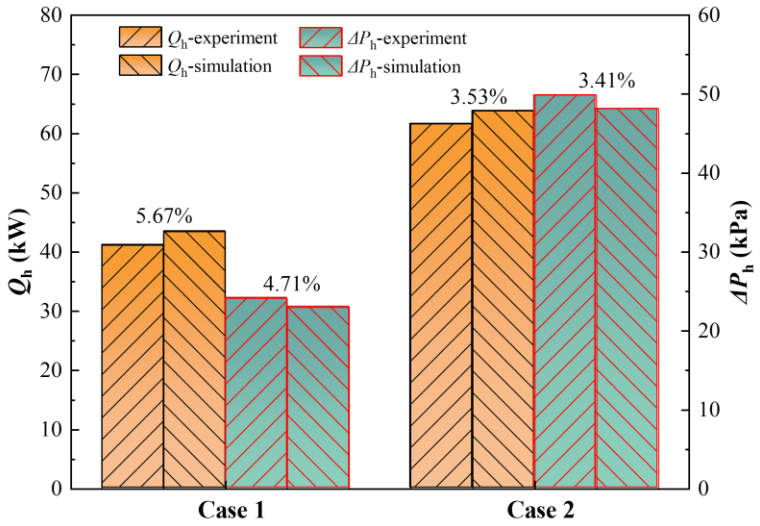

Figure 4. Comparison of Q_h and ΔP_h between simulation results and experimental results in Ref. [58] under the conditions of Case1 and Case2. (Case1: $T_{h,in}$ = 351.6 K, $T_{c,in}$ = 294.1 K, $\dot{m}_{h,in}$ = 0.27 g/s, $\dot{m}_{c,in}$ = 0.67 g/s, P_h = 8.2 MPa and P_c = 0.24 MPa. Case2: $T_{h,in}$ = 381.4 K, $T_{c,in}$ = 295.5 K, $\dot{m}_{h,in}$ = 0.35 g/s, $\dot{m}_{c,in}$ = 0.91 g/s, P_h = 8.2 MPa and P_c = 0.24 MPa.)

3.3. Validation of coupled heat transfer between LBE and CO_2-based mixtures

The thermophysical properties of binary mixtures of CO_2 with propane, krypton and xenon are determined from the NIST REFPROP 9.1 database, and these mixtures exhibit good chemical stability at elevated temperatures [59]. Figure 5 shows the variations of thermophysical properties with temperature for pure CO_2 and the mixtures in the range of 600-800 K. Here, the increase in temperature of the mixture significantly reduces its density, while the specific heat at constant pressure, thermal conductivity and viscosity increases monotonically.

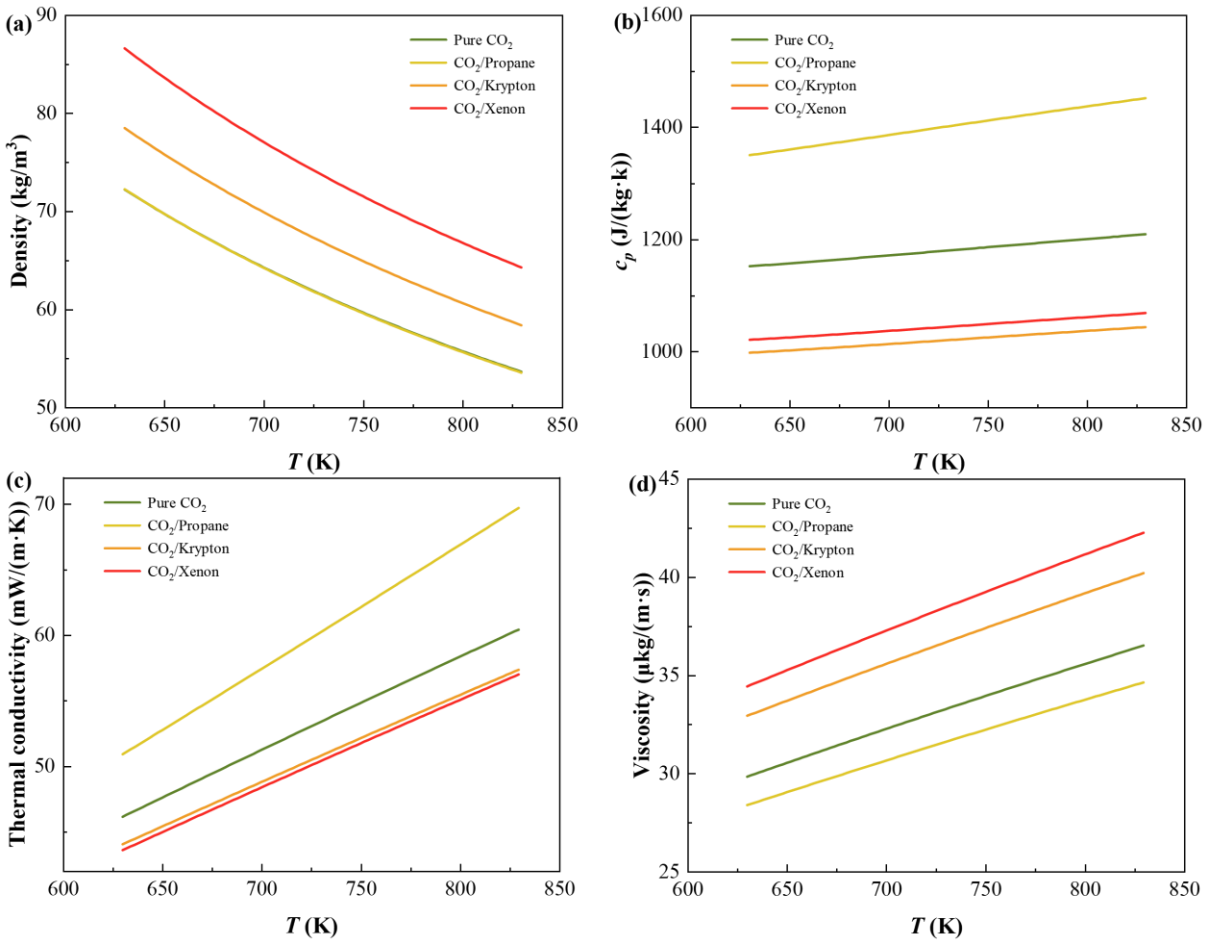

Figure 5. Thermophysical properties of CO_2-based mixtures with a CO_2/additive mole ratio of 9:1: (a) density, (b) specific heat at constant pressure, (c) thermal conductivity, and (d) viscosity.

To validate the effectiveness of the compiled UDF in invoking the Pr_t model for LBE, two comparison cases were simulated. Here, for CO_2-propane mixture with mole ratio of 8:2, the outlet pressure is 8.5 MPa and the inlet temperature is 650 K; for LBE, the inlet temperature is 800 K. The convective heat transfer coefficients and pressure drops in both hot and cold channels were compared between using the default constant $Pr_t = 0.85$ in ANSYS Fluent and the UDF-based implementation. As shown in Figure 6, when the default value $Pr_t = 0.85$ was applied on the LBE, the predicted convective heat transfer coefficient is higher than that predicted when using the model from Liu et al. [54]. This observation is consistent with the comparison of *Nu* under different Pr_t models which was conducted by Liu et al. [54].

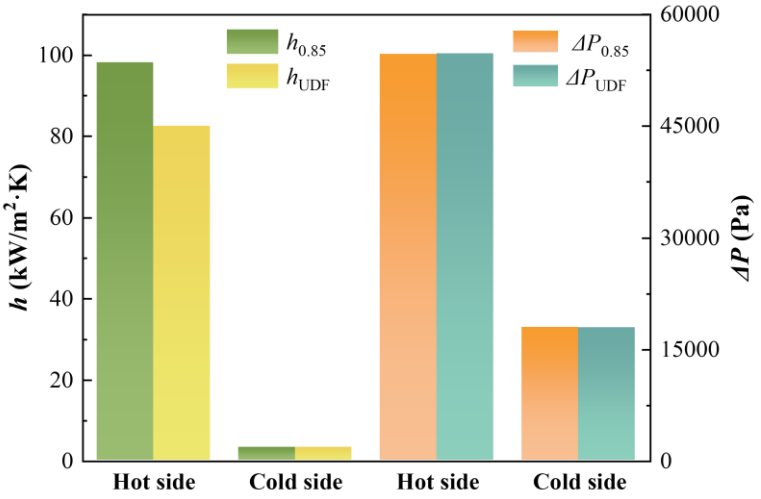

Figure 6. Heat transfer coefficient h and pressure drop ΔP for CO_2-propane mixture with mole ratio of 8:2: simulation results with constant $Pr_t = 0.85$ and UDF-based Pr_t model (Liu et al. [54]).

4. Results and discussion

4.1. Comparison of basic characteristics among different CO_2-based mixtures

The outlet temperature and pressure drop of both channels in a heat exchanger are key metrics for assessing thermal-hydraulic performance. Figure 7(a) and (b) present the outlet temperature and pressure drop of pure CO_2 and the various CO_2-based mixtures at different mole fractions. It is observed that under the operating conditions of $T_{h,in} = 800$ K, $v_{h,in} = 1.5$ m/s, $T_{c,in} = 650$ K and $\dot{m}_{c,in} = 1.15$ g/s, as compared to pure CO_2, the addition of propane exerts the most pronounced effect on outlet temperature, reducing the $T_{h,out}$ by up to 18.1 K. In contrast, the incorporation of xenon and krypton produces an opposite trend for $T_{h,out}$, leading to the increase of 19.1 K and 13.7 K, respectively. This indicates a reduction in heat transfer effectiveness between the primary and secondary loops. As shown in Figure 5, the incorporation of propane enhances both specific heat capacity and thermal conductivity of the mixture. This improvement augments the energy absorption capacity of the working fluid, thereby improving its overall heat transfer performance and reducing $T_{h,out}$. Conversely, adding gases such as krypton and xenon reduces the thermal transport capability of the cold fluid because of its low thermal conductivity. This diminishes the driving potential for interfacial heat transfer, ultimately elevating $T_{h,out}$.

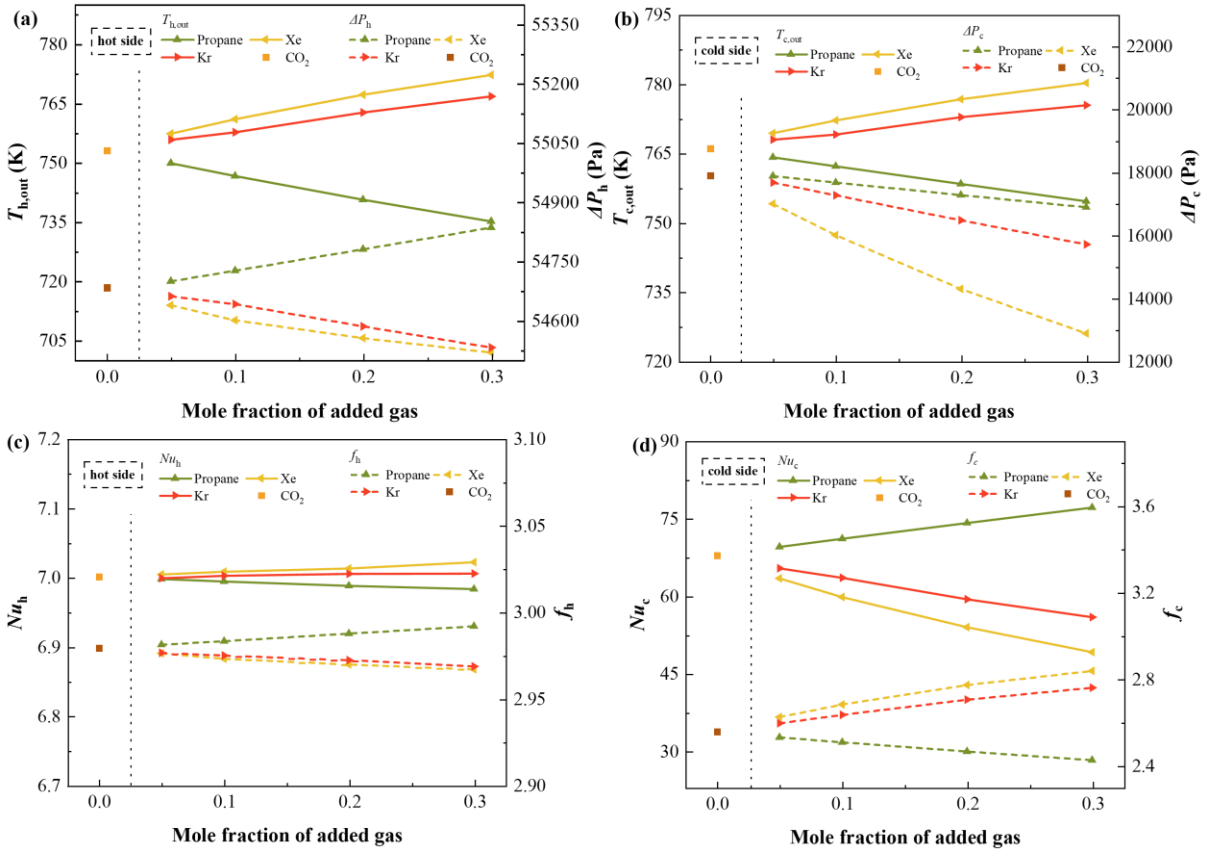

Figure 7. Effects of different mixtures on various flow and heat transfer parameters: (a) hot-side outlet temperature $T_{h,out}$ and pressure drop ΔP_h, (b) cold-side outlet temperature $T_{c,out}$ and pressure drop ΔP_c, (c) hot-side Nu_h and f_h, and (d) cold-side Nu_c and f_c. Here: $T_{h,in}$ = 800 K, $v_{h,in}$ = 1.5 m/s, $T_{c,in}$ = 650 K, and $\dot{m}_{c,in}$ = 1.15 g/s.

The addition of propane decreases the outlet temperature in cold channel $T_{c,out}$, whereas the incorporation of krypton and xenon leads to an increase in $T_{c,out}$. This trend is consistent with the variations observed on the hot side and can be primarily attributed to differences in the thermophysical properties of the mixtures. Specifically, the addition of propane enhances the specific heat capacity of the mixture, implying that the mixture absorbs more heat for each unit temperature rise. Consequently, the reduced $T_{c,out}$ indicates an enhancement in heat transfer rate, which further intensifies with higher propane mole fractions. Specifically, for pure CO_2, the heat exchange amount is 150.6 kW, whereas the heat exchange amount reaches 209.5 kW for CO_2-propane mixture. The total heat exchange amount can increase by up to 39% compared to pure CO_2. In contrast, the blending of krypton or xenon reduces the heat capacity of mixture, thereby increasing $T_{h,out}$ under the same thermal load on cold channel.

Figure 7(c) and (d) shows the variations in the Nusselt number *Nu* and Darcy friction factor *f* for these four working fluids at various mixing ratios. Under the operating conditions of $T_{h,in}$ = 800 K, $T_{c,in}$ = 650 K, $v_{h,in}$ = 1.5 m/s, and $\dot{m}_{c,in}$ = 1.15 g/s, the addition of propane slightly

decreases the hot-side Nu_h. As the mole fraction of propane increases, Nu_h also decreases slightly. This is mainly because the enhanced heat absorption in the cold channel modifies the temperature distribution in the PCHE and lowers the LBE temperature. The decrease in LBE temperature increases its viscosity, which tends to reduce the hot-side *Re* under the same inlet velocity. As a result, the hot-side convective transport is slightly weakened, leading to a slight decrease in Nu_h. Meanwhile, the increased viscosity strengthens the near-wall viscous effect, resulting in a slight increase in the hot-side friction factor f_h. In contrast, with the addition of xenon or krypton, the hot-side Nu_h increases slightly, whereas f_h decreases.

For the cold side, as the mole fraction of propane increases from 0 to 0.30, the cold-side Nu_c increases substantially, with a maximum enhancement of approximately 14%. This enhancement is mainly associated with the lower viscosity of the CO_2-propane mixture, which increases *Re* in the channel under the same inlet mass flow rate and strengthens near-wall convective transport. Conversely, adding xenon and krypton decreases Nu_c as the mole fraction increases, with the maximum reductions reaching 28% and 18%, respectively. This is mainly associated with the reduced *Re* and weakened convective transport of the corresponding mixtures. Moreover, as the mole fraction of propane increases, the cold-side friction factor f_c decreases slightly, with a maximum reduction of 5.3% as compared with pure CO_2. This reduction is mainly associated with the decrease in viscosity and the corresponding change in near-wall momentum transport. Conversely, the addition of xenon and krypton increases f_c as the mole fraction rises, with maximum increases of 11% and 7.8%, respectively. To assess the impact of mixture on PCHE performance, the U_{mix}/U_{CO2} ratio is used as the heat transfer performance criterion (see Eq. (9)). Here, *U* denotes the overall heat transfer coefficient, the subscript m represents CO_2-based mixtures while subscript c represents pure CO_2.

Figure 8 shows that adding propane increases U_{mix}/U_{CO2} by up to 40% compared to that of pure CO_2, whereas krypton and xenon reduce it by 36% and 27%, respectively. This result further confirms that propane plays a significant role in enhancing heat transfer.

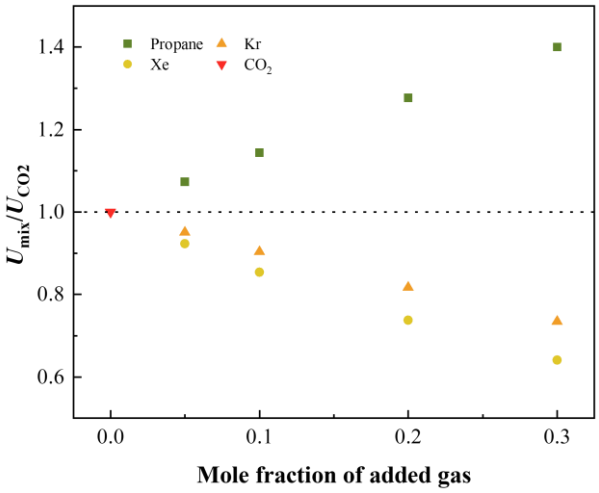

Figure 8. Effect of different mixtures on U_{mix}/U_{CO2}.

As discussed above, for the CO_2-propane cases, the heat-transfer enhancement is primarily associated with the reduction in mixture density and viscosity. Under the same inlet mass flow rate, the lower viscosity increases *Re* in the channel and strengthens near-wall convective transport, leading to an increase in *Nu*. Although thermal conductivity also varies with propane addition and contributes to *h*, the *Nu* trend cannot be explained by thermal conductivity alone without considering the *Re* and *Pr* effects and convective transport behaviour.

In contrast, for the CO_2-Kr and CO_2-Xe cases, the increase in viscosity reduces *Re* and weakens convective transport under the investigated conditions, resulting in lower *Nu* compared with pure CO_2. Regarding flow resistance, the variation in *f* is mainly associated with viscosity and near-wall momentum transport. The increased viscosity of the CO_2-Kr and CO_2-Xe mixtures leads to stronger viscous effects and higher *f*, whereas the lower viscosity of the CO_2-propane mixture contributes to a slight decrease in *f*.

4.2. Heat transfer and flow characteristics of LBE and CO_2-propane mixture

4.2.1. Effect of inlet velocity

Figure 9 shows the temperature distribution across both sides of the semi-circular channel at four axial positions (x = 40 mm, 80 mm, 120 mm, and 160 mm) under various operating conditions. In Figure 9, the upper and lower cross-sections represent the LBE side and the CO_2-propane mixture side. It is observed that the increase of the mole fraction of propane reduces the temperature of LBE significantly. Furthermore, the temperature gradients on both sides exhibit distinct differences, with the temperature distribution in the mixture flow path becoming increasingly non-uniform, exhibiting clear thermal stratification.

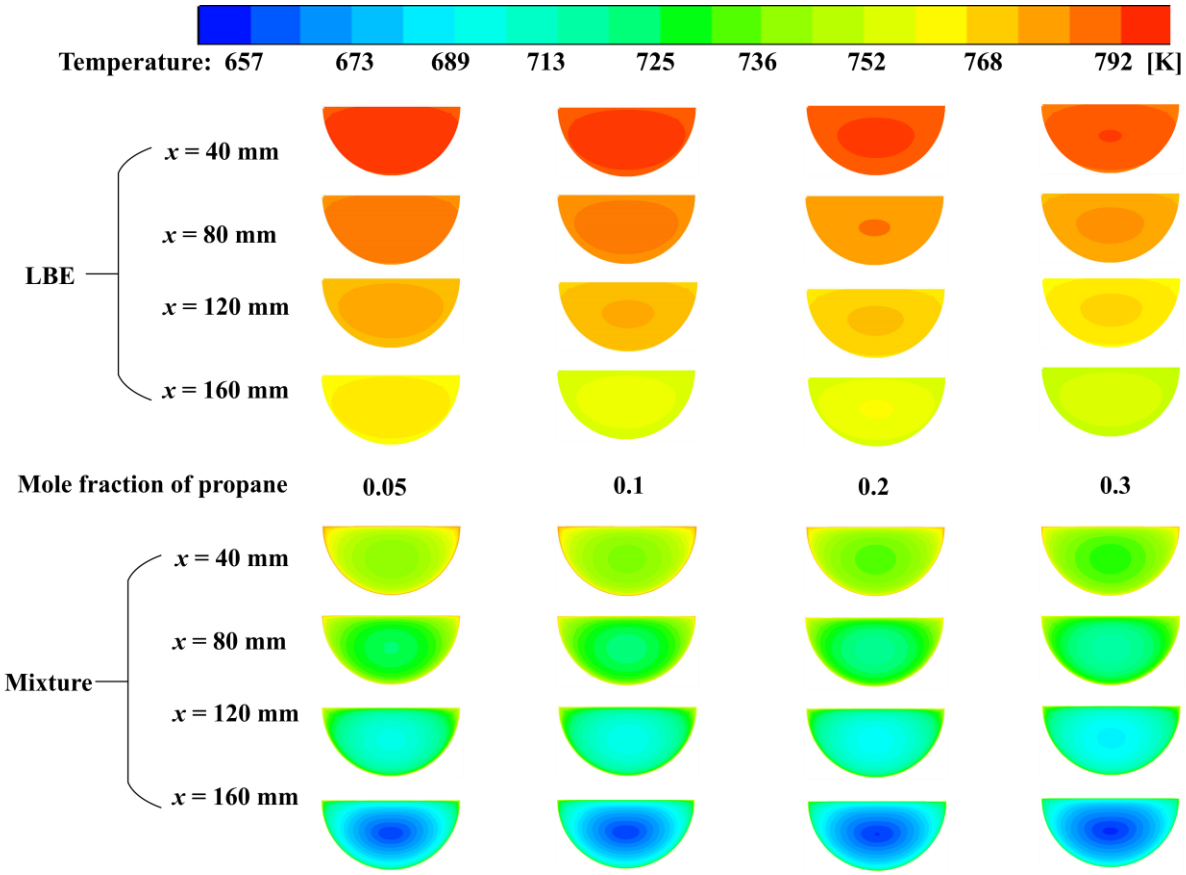

Figure 9. Temperature contours at four axial sections (x = 40, 80, 120, 160 mm) under $v_{h,in}$ = 1.5 m/s, $T_{h,in}$ = 800 K, $T_{c,in}$ = 650 K, and $\dot{m}_{c,in}$ = 1.1 g/s: LBE (top) and CO_2-propane mixtures (bottom) with different mixing ratios (α = 0.05, 0.10, 0.20, 0.30).

In Figure 10(a) and (b), the variations of the *Nu* and *f* in both the hot and cold channels of the straight-channel PCHE are analysed under different LBE inlet velocities. When $T_{h,in}$ = 800 K, $T_{c,in}$ = 650 K, and $\dot{m}_{c,in}$ = 1.1 g/s, as the mole fraction of propane increases from 0.05 to 0.30, the *Nu* of the mixture increases by a maximum of 13% at a constant LBE inlet velocity, whereas the *f* decreases by up to 3.7%. This is mainly because blending propane increases the mixture's thermal conductivity and decreases its viscosity. These changes enhance convective heat transfer and reduce flow resistance, manifesting as an increase in *Nu* and a decrease in *f*. Additionally, the addition of propane leads to only a marginal rise in *Nu* and *f* on the hot channel. This is because the thermophysical properties of the LBE remain unchanged, while the enhanced heat transfer performance on the cold channel increases the thermal flux density. This increases the temperature gradient slightly and promotes convective heat transfer in the hot channel. As the LBE inlet velocity increases from 1 m/s to 1.75 m/s, under the same mole fraction of propane, the *Nu* of the mixture shows a decreasing trend, with a maximum reduction of 2.1%, whereas the *f* increases slightly. On the hot channel, the *Nu* increases slightly with the velocity increasing. This is primarily because the higher flow velocity intensifies the

turbulence, thus strengthening the convective heat transfer.

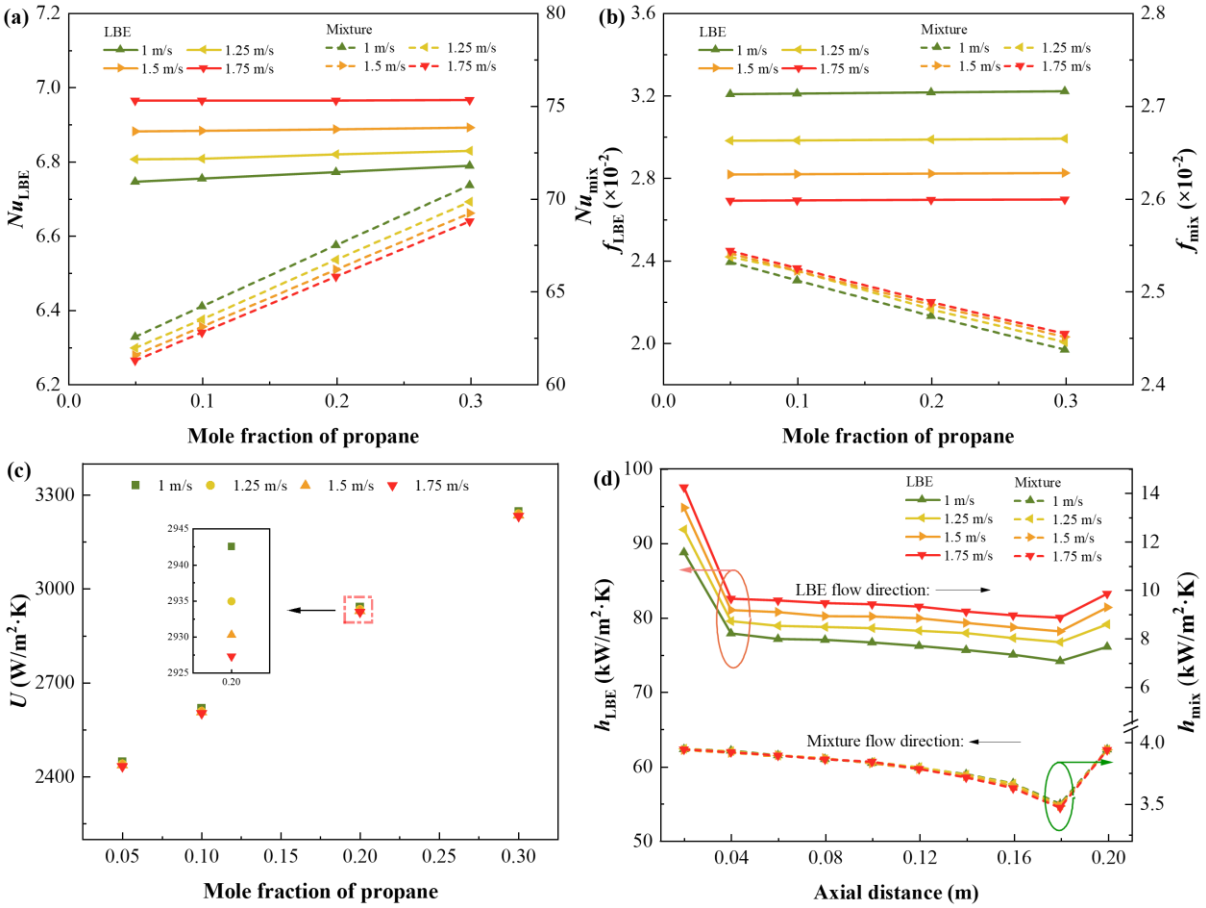

Figure 10. Flow and heat transfer parameters for various LBE inlet velocities: (a) *Nu*, (b) *f*, (c) *U*, and (d) *h*.

Figure 10(c) shows the variation in the overall heat transfer coefficient *U* under different LBE inlet velocities. It is observed that increasing the mole fraction of propane significantly enhances *U* in the PCHE, with a maximum enhancement of 25%. At the same propane mole fraction, when the LBE inlet velocity decreases from 1.75 m/s to 1.0 m/s, *U* increases slightly by approximately 0.5% under the investigated conditions. Due to the high thermal conductivity of LBE, the hot-side thermal resistance remains relatively small compared with the cold-side thermal resistance. Therefore, changing the LBE inlet velocity within the investigated range has only a limited influence on the total thermal resistance. A lower LBE inlet velocity increases the residence time of the hot fluid and modifies the wall temperature distribution. Under the investigated conditions, this coupled changes in wall temperature distribution and local heat transfer lead to a slight decrease in the overall effective thermal resistance, resulting in a modest increase in the overall heat transfer coefficient.

To further investigate the local area-averaged convective heat transfer coefficient, cross-

sections were sampled every 20 mm along the flow direction. Under constant flow conditions of the mixture (mole ratio at 8:2), the variation in local heat transfer coefficient was investigated as the LBE inlet velocity increased from 1.0 m/s to 1.75 m/s. As shown in Figure 10(d), increasing LBE velocity consistently raises the hot-side coefficient, with the strongest augmentation near the inlet and a peak of approximately 100 kW/(m^2·K). This arises from the increasing Reynold's number and intensified turbulence, which accelerate near-wall momentum and energy exchange. The corresponding increase in wall heat flux further reinforces the local driving force. In contrast, the cold-side coefficient shows minimal variation with LBE velocity increasing, remaining 3.5-4.0 kW/(m^2·K) with slight axial fluctuations. This suggests that the cold-side thermal resistance dominates in the heat transfer process and is not substantially mitigated by an increase in the hot-side velocity.

4.2.2. Effect of inlet temperature

Figure 11(a) and (b) shows the *Nu* and *f* in both channels under varying LBE inlet temperatures. For $v_{h,in}$ = 1.5 m/s, $T_{c,in}$ = 650 K, and $\dot{m}_{c,in}$ = 1.1 g/s, as $T_{h,in}$ increases from 775 K to 850 K, the *Nu* of mixture shows a slight decreasing trend with a constant propane mole fraction, with a maximum reduction of 5.1%, while the *f* increases by 3.5%. On the hot channel, the *Nu* increases slightly while *f* decreases by 2.1%. This phenomenon is attributed to the decreasing viscosity of the LBE, which enhances the *Re*, thereby increasing the *Nu*. Simultaneously, the elevated temperature reduces the fluid viscosity, thus reducing the f_h. On the cold channel, the decrease in *Nu* and the increase in *f* are primarily due to the rise in mixture temperature. The rising temperature leads to a higher viscosity, thereby weakening the convective heat transfer capability and simultaneously elevates flow resistance.

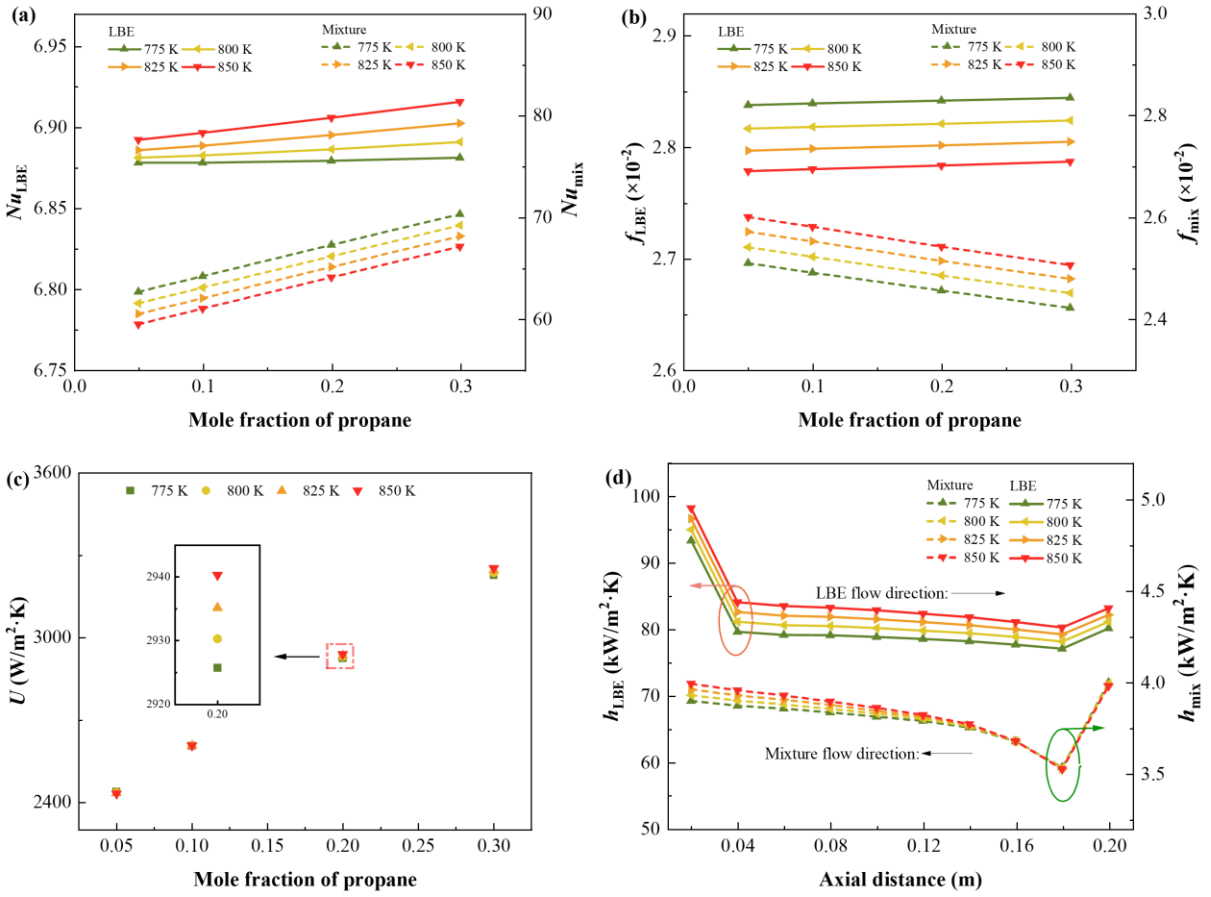

Figure 11. Flow and heat transfer parameters for various LBE inlet temperatures: (a) *Nu*, (b) *f*, (c) *U*, and (d) *h*.

Figure 11(c) shows the variation in *U* of the straight-channel PCHE under different LBE inlet temperatures. It can be observed that within the LBE inlet temperature range of 775 K to 850 K, increasing the inlet temperature results in only a slight increase in *U* at the same mole fraction. Figure 11(d) shows *h* distributions for both fluids under different hot-channel temperature conditions, with the CO_2-propane mixture fixed at 8:2. Increasing $T_{h,in}$ increases the temperature difference and enhances the coefficient in hot channel over the entire length, which reflects a stronger driving potential and intensified near-wall transport. For the cold side, as the LBE temperature increases, the heat transfer coefficient of mixture exhibits a gradual upward trend, with the difference becoming more pronounced near the outlet section.

4.2.3. Effect of CO_2-propane mixture inlet flow rate

Figure 12(a) and (b) shows the variations in *Nu* and *f* for both channels under different cold-side mass flow rates $\dot{m}_c$ (ranging from 1.1 g/s to 2.0 g/s). For $T_{h,in}$ = 800 K, $v_{h,in}$ = 1.5 m/s, and $T_{c,in}$ = 650 K, with the same mole fraction of propane, increasing $\dot{m}_c$ leads to a notable enhancement in the *Nu* of mixture. Compared to $\dot{m}_c$ = 1.1 g/s, the case of $\dot{m}_c$ = 2.0 g/s increases the flow *Nu* by 44%. This enhancement is primarily due to higher velocity and turbulence

intensity, thereby improving heat transfer. Meanwhile, the mixture f decreases with increasing $\dot{m}_c$, with a maximum reduction of 16%, attributed to the higher velocity that effectively reduces the relative flow resistance. For the LBE, both the Nu and f increase with $\dot{m}_c$ (with f increasing slightly) because the temperature difference between LBE and CO_2-propane mixture increases, which improves overall heat transfer and further enhances LBE's heat transfer capacity.

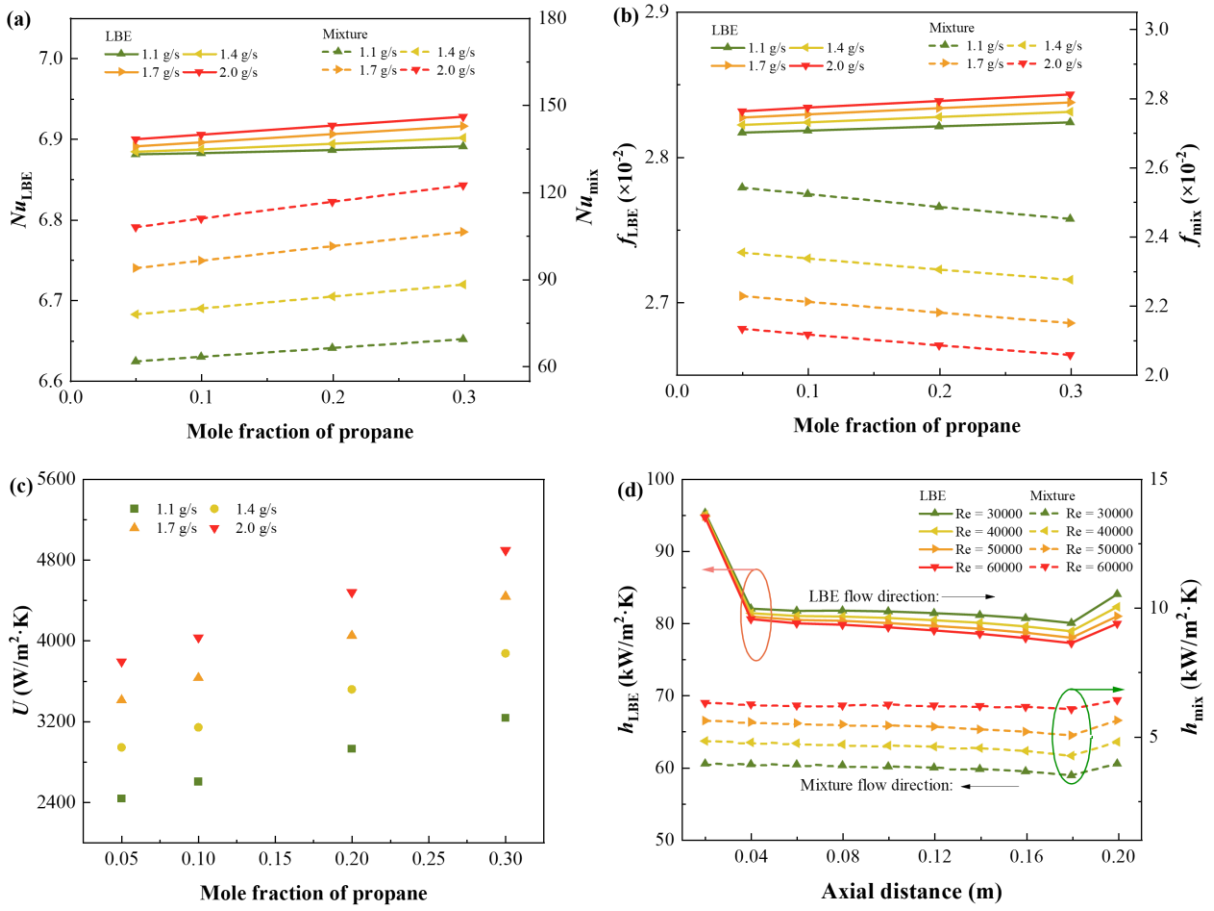

Figure 12. Flow and heat transfer parameters for various CO_2-propane mixture mass flow rates: (a) Nu, (b) f, (c) U, and (d) h.

Figure 12(c) shows the variation in U of the PCHE under different $\dot{m}_c$. It is observed that an increase of $\dot{m}_c$ from 1.1 g/s to 2.0 g/s increases U by 51% at the same mole fraction. Figure 12(d) reveals that h in cold channel improves significantly with the Re increasing, while that of LBE decreases slightly. This implies an enhancement in heat transfer capability of mixture. Compared to Re = 30,000, the h in the cold channel increases significantly when Re = 60,000. This improvement would be expected to arise at higher mass flow rates and Re, which intensify turbulence and increase near-wall mass and heat transport (see Figure S2), thereby reducing the mixture's thermal resistance.

4.2.4. Effect of CO_2-propane mixture inlet temperature

Figure 13(a) and (b) shows the variations of Nu and f for both channels when using CO_2-propane mixtures under different inlet temperatures. For $T_{h,in}$ = 800 K, $v_{h,in}$ = 1.5 m/s, and $\dot{m}_{c,in}$ = 1.1 g/s, as $T_{c,in}$ increases from 600 K to 675 K, the Nu of mixture shows a decreasing trend at the same propane mole fraction, with a maximum reduction of 1.5%. This variation is primarily due to the decrease in the λ and c_p of the mixture, thus weakening the thermal energy exchange capacity of the mixture. Meanwhile, the mixture's f also decreases with a maximum reduction of 2.7%. This is attributed to the decrease in fluid viscosity at higher temperature, which diminishes the friction between the fluid and the wall, thus lowering the flow resistance. On the hot channel, the Nu also exhibits a slight decreasing trend, with a maximum reduction of 1.0%. Although higher temperatures typically increase the thermal flux, the aforementioned changes in the mixture's thermophysical properties partially inhibit overall heat transfer performance. Similarly, the f of LBE decreases slightly due to the reduction in viscosity, which leads to lower flow resistance.

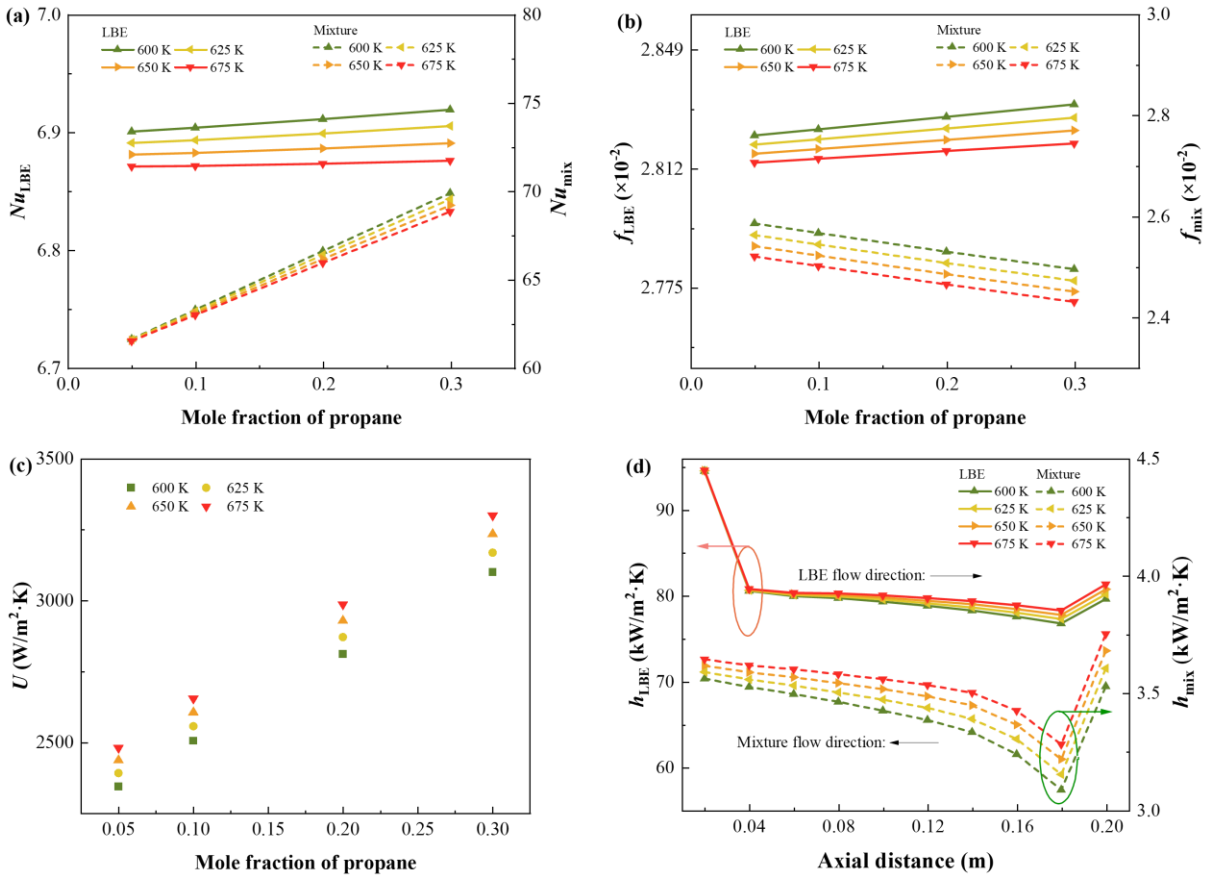

Figure 13. Flow and heat transfer parameters for various CO_2-propane mixture inlet temperatures: (a) Nu, (b) f, (c) U, and (d) h.

Figure 13(c) demonstrates that within the inlet temperature range of 600 K to 675 K, U

exhibits a notable enhancement as the inlet temperature of the mixture rises at the same mole fraction. Furthermore, the increase in $T_{c,in}$ leads to a reduction in the fluid density and a higher velocity, which in turn enhances the turbulence intensity and turbulent kinetic energy. Accordingly, the enhanced turbulent kinetic energy improves heat transfer capability near the wall and ultimately increases the mixture's heat transfer coefficient, as shown in Figure 13(d). In addition, the λ of the CO_2-propane mixture increases slightly, which further enhances its heat transfer capacity. For the LBE, although the flow velocity remains constant, its thermal conductivity increases with temperature changes, thereby enhancing heat transfer performance.

4.2.5. Effect of CO_2-propane mixture pressure

Figure 14(a) and (b) shows the variations in *Nu* and *f* for both channels under different pressure conditions of the CO_2-propane mixture (ranging from 8.5 MPa to 18.5 MPa). For the operating conditions of $T_{h,in}$ = 800 K, $T_{c,in}$ = 650 K, $v_{h,in}$ = 1.5 m/s, and $\dot{m}_{c,in}$ = 1.1 g/s, as the pressure of CO_2-propane increases, the *Nu* of mixture shows a decreasing trend at a constant mole fraction of propane, with a maximum reduction of 2.5%. Additionally, the *f* of mixture increases, with a maximum increase of 3.2%. This is because higher system pressure raises the density and reduces the velocity in the cold channel, which weakens the turbulence intensity. Meanwhile, the effect of fluid viscosity becomes more prominent, resulting in an increase in the *f*. The *Nu* of LBE remains relatively unaffected with pressure changes. This is because the flow velocity and temperature of the LBE are relatively stable, and its thermophysical properties are less sensitive to pressure.

Figure 14(c) shows the overall heat transfer coefficient in the pressure range from 8.5 MPa to 18.5 MPa. Increasing the pressure enhances the overall heat transfer coefficient by 1.5% at the same mole fraction. Although Nu_c decreases slightly with increasing pressure due to the reduction in Re and turbulence intensity, *U* is governed by the total thermal resistance rather than solely by turbulence intensity. Compared with P_c = 8.5 MPa, the thermal conductivity and specific heat capacity at P_c = 18.5 MPa are higher by up to 5.1% and 2.0%, respectively, which affect the near-wall transport process and convective heat transfer behaviour and thus leads to a reduction in cold-side thermal resistance. Since the thermal resistance of the present PCHE is primarily dominated by the cold side, the reduction in cold-side resistance results in a decrease in the overall thermal resistance. As a result, the overall thermal resistance decreases under high-pressure conditions, leading to an increase in *U*. As shown in Figure 14(d), as the pressure increases from 8.5 MPa to 18.5 MPa, the *h* in cold channel shows a gradual increase along the entire flow path, from 3.79 kW/(m^2·K) to

3.93 kW/(m^2·K). Meanwhile, the h of LBE shows a slight decrease and remains relatively stable throughout the heat transfer process. Therefore, the pressure of CO_2-propane mixtures exerts a stronger influence on the heat transfer performance in cold channels, whereas no significant impact is observed for the LBE (hot channel).

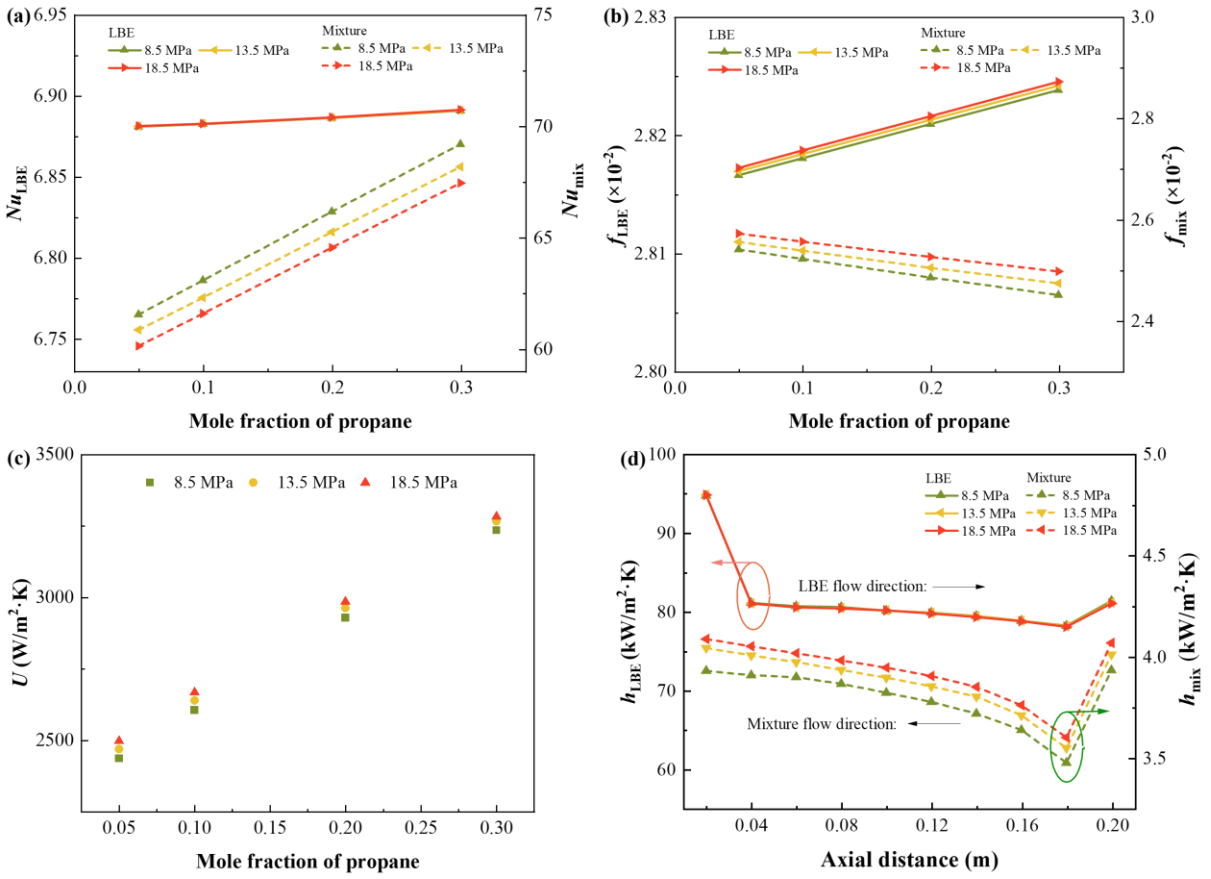

Figure 14. Flow and heat transfer parameters for various CO_2-propane mixture pressures: (a) *Nu*, (b) *f*, (c) *U*, and (d) *h*.

4.3. Correlations for both LBE and CO_2-propane mixture

To assess the accuracy and applicability of flow and heat transfer correlations for both fluids in straight-channel PCHEs, the correlations listed in Table 2 and 3 were selected to predict the *Nu* and *f* for LBE and CO_2-propane mixture, respectively. The prediction accuracy of each correlation was evaluated by comparing the deviation between the predicted values and the simulation results. The deviation is used for evaluation and is defined by:

$$deviation = \frac{R_{pre} - R_{sim}}{R_{sim}} \times 100\% \quad (12)$$

where R_{pre} denotes the predictive results calculating by typical correlations under the same dimensionless number in this study, and R_{sim} denotes the simulation results in this study.

496 **Table 2.** Summary of correlations for heat transfer characteristics.

Ref.	Correlations	Working conditions
Skupinski et al. [60]	$Nu = 4.82 + 0.0185Pe^{0.827}$	LBE; *Re*: 10^4-5×10^6
Kirillov et al. [61]	$Nu = 4.5 + 0.018Pe^{0.8}$	LBE; *Pe*: 0-2,000
Sleicher et al. [62]	$Nu = 6.3 + 0.0167Pr^{0.08}Pe^{0.85}$	Liquid metal; *Pr*: 0.004-0.1
Fu et al. [41]	$Nu = 6.3 + 0.018Pe^{0.8}$	LBE; *Pe*: 240-310
Zhou et al. [47]	$Nu = 0.02986\times Re^{0.77734}\times Pr^{0.30678} \times\left(\frac{\rho_w}{\rho_b}\right)^{0.34962}\times\left(\frac{\mu_w}{\mu_b}\right)^{-0.5639}\times\left(\frac{c_{pw}}{c_{pb}}\right)^{0.347}\times\left(\frac{\lambda_w}{\lambda_b}\right)^{-0.02617}$	CO_2-based mixture; *Re*:13826-31578
Meshram et al. [57]	$Nu = 0.0514Re^{0.76}Pr^{0.55}$	sCO_2; Straight Channel *D* = 2 mm
Bishop et al. [63]	$Nu = 0.0069Re^{0.9}Pr^{0.66}\left(\frac{\rho_w}{\rho_b}\right)^{0.43}\left(1+\frac{2.4}{L/D_e}\right)$	sCO_2; T_b: 555-800 K
Ren et al. [18]	$Nu = 0.01882Re^{0.82}Pr^{0.5}\left(\frac{\rho_b}{\rho_w}\right)^{-0.3}\left(\frac{\mu_b}{\mu_w}\right)^{0.2887}$	sCO_2; *Re*: 11,000-70,000

497 **Table 3.** Summary of correlations for flow characteristics.

Ref.	Correlations	Working conditions
Filonenko et al. [64]	$f = \left(1.82\lg Re - 1.64\right)^{-2}$	supercritical fluid; *Re*: 4,000-10^{12}
Liu et al. [51]	$f = \left(2.266\lg Re - 3.6\right)^{-2}$	LBE; *Re*: 2,800-12,000
Meshram et al. [57]	$f = 0.8385Re^{-0.5978} + 0.00331$	sCO_2; straight channel *D*=2 mm
Zhou et al. [47]	$f = 0.09579\times Re^{-0.26093}\times\left(\frac{\rho_w}{\rho_b}\right)^{-0.19607}\times\left(\frac{\mu_w}{\mu_b}\right)^{0.22885} \times\left(\frac{c_{pw}}{c_{pb}}\right)^{-0.03687}\times\left(\frac{\lambda_w}{\lambda_b}\right)^{0.09512}$	CO_2-based mixture; *Re*: 14,000-32,000
Kirillov et al. [65]	$f = \left(1.82\lg Re - 1.64\right)^{-2}\left(\frac{\rho_w}{\rho_b}\right)^{0.4}$	supercritical water; *Re*: 8×10^4-1.5×10^6

4.3.1. Typical LBE correlations

In this work, typical correlations were used to predict the *Nu* and *f* of LBE flowing horizontally within the semi-circular channel. As shown in Figure 15(a) and (b), the deviation between the numerical simulation results for *Nu* of LBE (Nu_h) and calculated values using the correlation developed by Skupinski et al. [60] is within ±15%, while that of correlation developed by Kirillov et al. [61] is mostly within ±20%. The numerical simulation results are generally higher than the predictions from both correlations. As shown in Figure 15(c) and (d), the deviation between the simulation results for the Nu_h and the predictions from the correlation developed by Sleicher et al. [62] is within ±9%, while that of correlation developed by Fu et al. [41] is within ±11%. The simulation results are generally lower than the predictions from the two correlations.

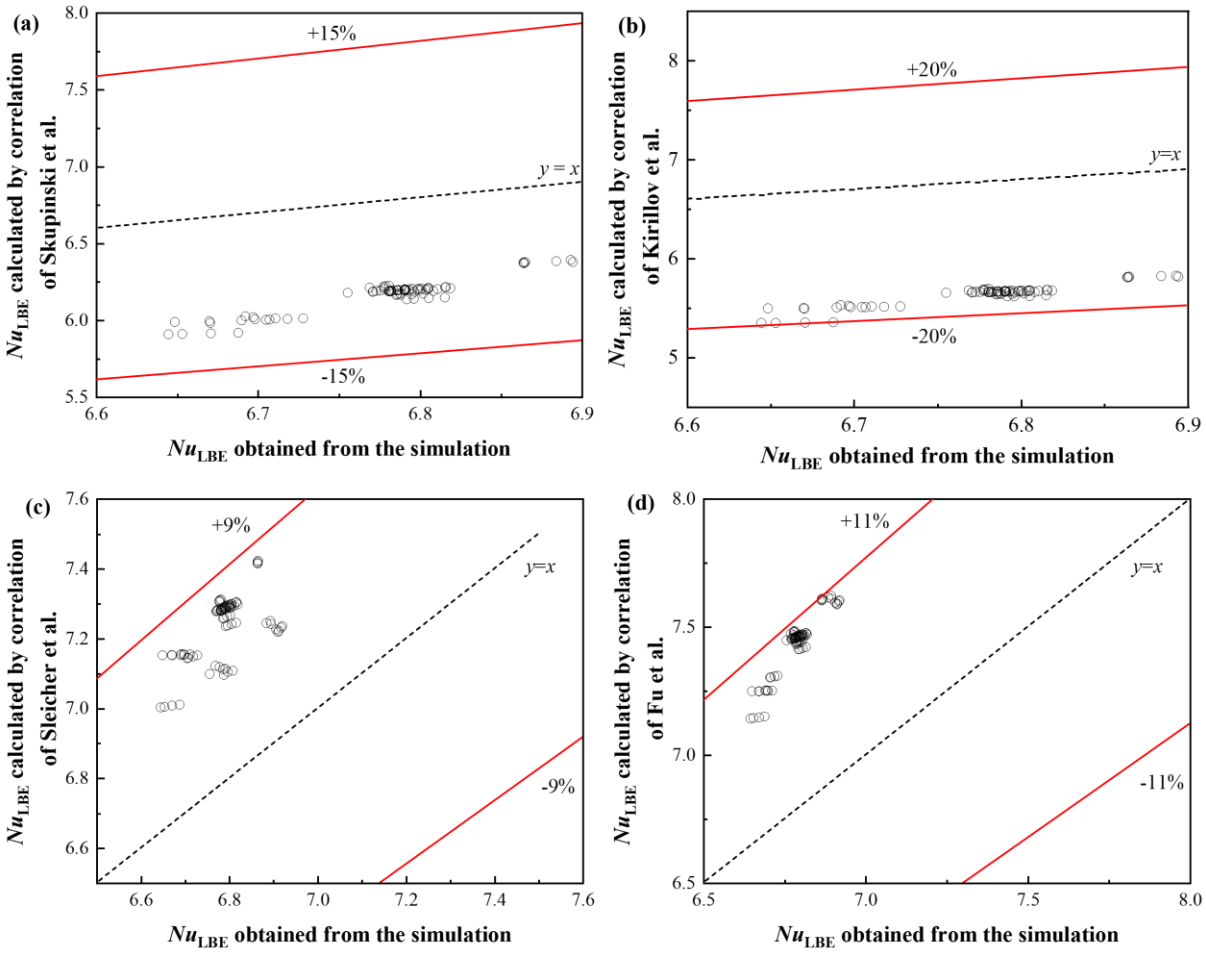

Figure 15. Comparison of LBE *Nu* between simulation results of this study and calculated values using typical correlations. The horizontal axis denotes the simulated *Nu*, while the vertical axis denotes the *Nu* calculated from different correlations: (a) Skupinski et al. [60], (b) Kirillov et al. [61], (c) Sleicher et al. [62], and (d) Fu et al. [41].

Although the friction factor correlation developed by Filonenko et al. is originally proposed for supercritical fluids, previous study [51] has shown that it also provides reasonably

accurate predictions for LBE under certain operating conditions. Thus, this study also applies this correlation to evaluate the *f* of LBE. As shown in Figure 16(a) and (b), the deviation between the simulation results for *f* of LBE and the predictions from the correlation developed by Filonenko et al. [64] is within ±5%. Additionally, the prediction deviation from that of the correlation developed by Liu et al. [51] is within ±10%. Overall, the simulation results are generally higher than the predictions from the correlations.

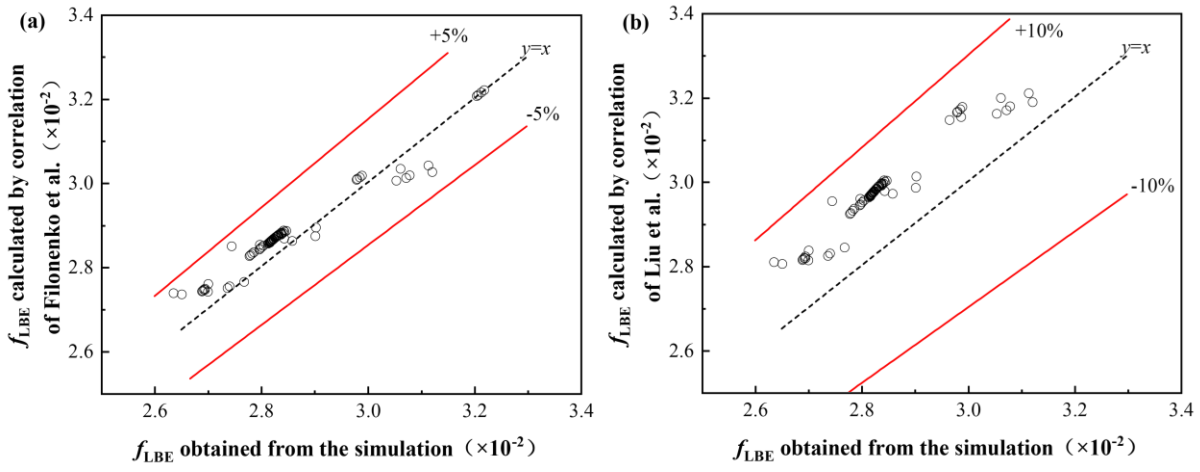

Figure 16. Comparison of LBE *f* between simulation results of this study and calculated values using typical correlations. The horizontal axis denotes the simulated *f*, and the vertical axis denotes the *f* calculated using different correlations: (a) Filonenko et al. [64], and (b) Liu et al. [51].

Therefore, for the LBE in hot channel, within under the LBE conditions in this study ($P_{h,out}$ = 0.1 MPa, $T_{h,in}$ = 775-850 K, and Pe_h = 309-515), it is advised to use the heat transfer correlation developed by Fu et al. [41] to predict *Nu* and the friction factor correlation developed by Filonenko et al. [64] to predict *f*.

4.3.2. Typical correlations and development of new correlations for CO_2-propane mixtures

As for the CO_2-propane mixture in the supercritical state, the pronounced changes in thermophysical properties must be considered in relation to the flow and heat transfer mechanism. Due to the high density gradient, low viscosity, and varying thermal conductivity of the mixture, this study employs the correlations developed by Filonenko et al. [64], Zhou et al. [47], Meshram et al. [57], and Kirillov et al. [65] to predict the *Nu* and *f*, respectively. As shown in Figure 17, the deviation between the simulation results for the *Nu* in mixture and the predictions using correlations developed Zhou et al. [47], Ren et al. [18], Meshram et al. [57], and Bishop et al. [63] is within ±15%, ±20%, ±70%, and ±20%, respectively. In Figure 18, the deviation between the simulation results for *f* of mixture and the predictions using correlations developed by Filonenko et al. [64], Zhou et al. [47], Meshram et al. [57], and Kirillov et al. [65]

is within ±10%, ±12%, ±20%, and ±11%, respectively. The inconsistency may stem from the cold channel parameters (Pr = 0.73-0.79, Re = 25,000-60,000) lying outside the applicable range of correlations. Additionally, the computational model and conditions in the correlations differ from those in this study. In comparison, the heat transfer correlation developed by Zhou et al. [47] has a deviation of less than 15%, demonstrating better predictive capability for the Nu of the mixture. The friction factor correlation developed by Filonenko et al. [64] demonstrates better predictive capability for the CO_2-propane mixture.

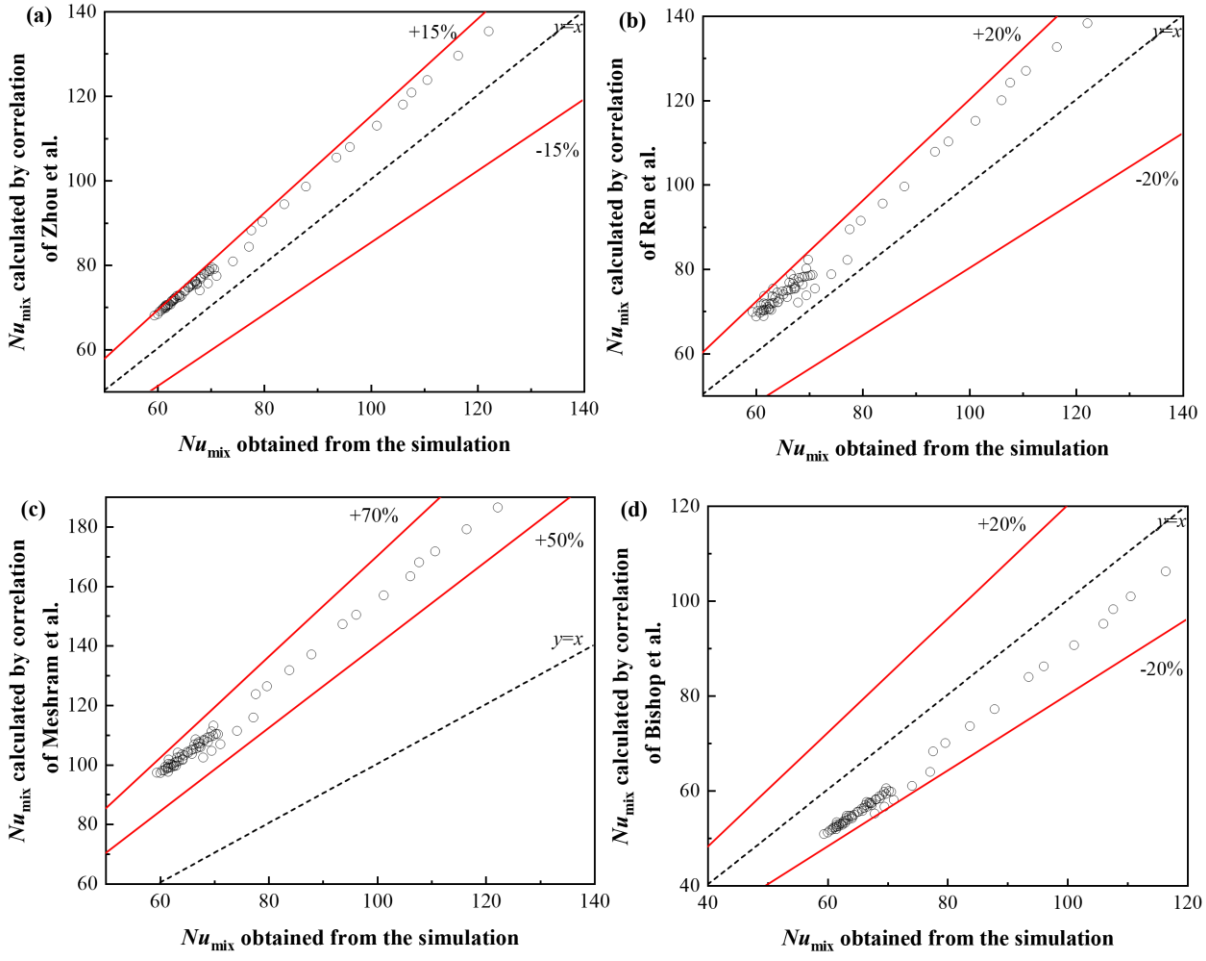

Figure 17. Comparison of CO_2-propane Nu between simulation results of this study and calculated values using typical correlations. The horizontal axis denotes the simulated Nu, and the vertical axis denotes the Nu calculated using different correlations: (a) Zhou et al. [47], (b) Ren et al. [18], (c) Meshram et al. [57], and (d) Bishop et al. [63].

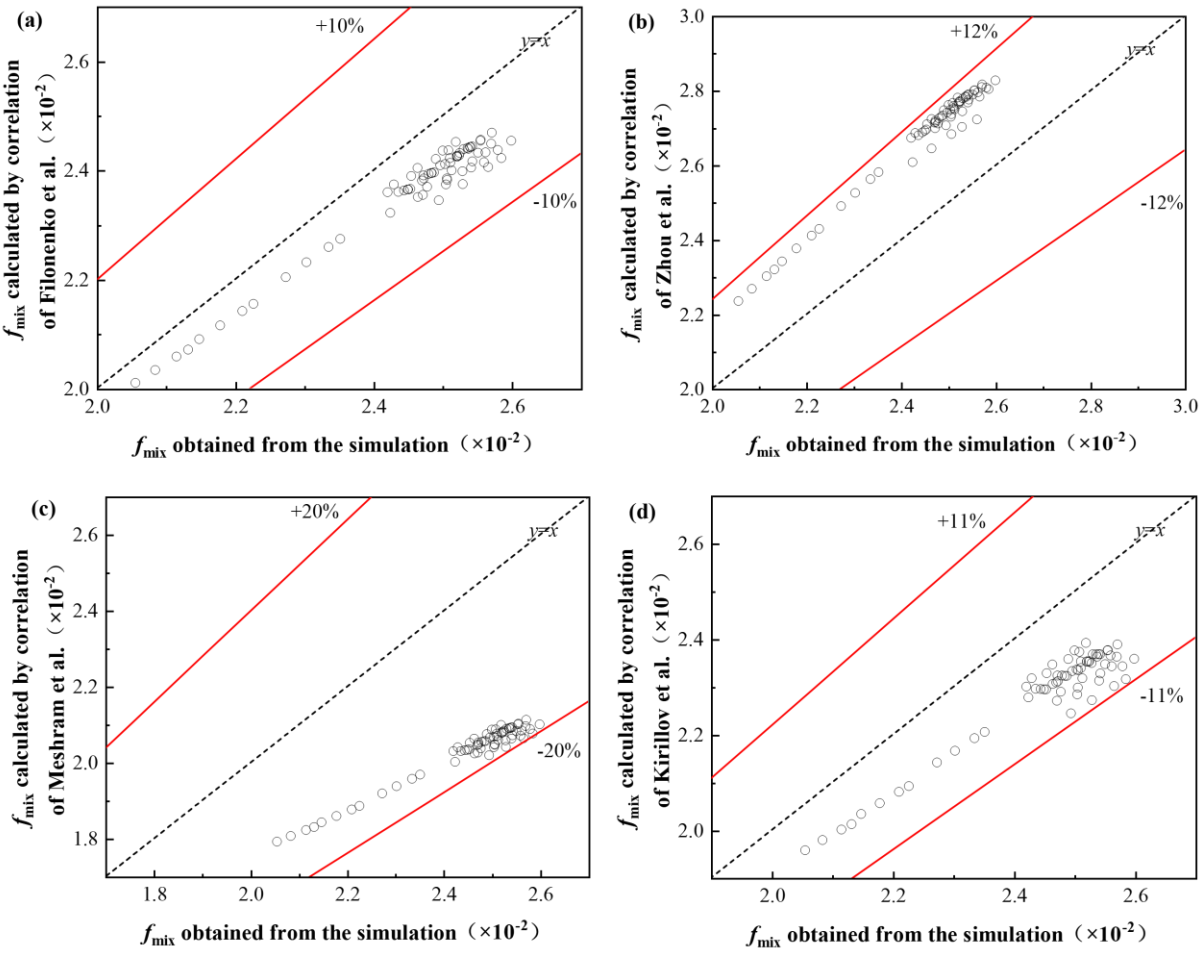

Figure 18. Comparison of CO_2-propane f between simulation results of this study and calculated values using typical correlations. The horizontal axis denotes the simulated f, and the vertical axis denotes the f calculated using different correlations: (a) Filonenko et al. [64], (b) Zhou et al. [47], (c) Meshram et al. [57], and (d) Kirillov et al. [65].

The evaluation of the selected Nu and f correlations reveals that their prediction results have limited applicability under the conditions of this study. Although they are within an acceptable range, the prediction accuracy still requires further improvement. To address this issue, the new correlations were developed based on simulation data in cold channel using MATLAB (Eqs. (13) and (14)). In the process of fitting, the influence of mixture's thermophysical properties was thoroughly considered, and the optimal values for each coefficient were determined through multiple iterations. The specific expressions are:

$$Nu_c = 0.02992 \cdot Re^{0.78695} \cdot Pr^{0.8783} \cdot \left(\frac{\lambda_w}{\lambda_b}\right)^{-2.502} \cdot \left(\frac{c_{pw}}{c_{pb}}\right)^{5.415} \tag{13}$$

$$f_c = 0.3238 \cdot Re^{-0.2533} \cdot \left(\frac{\rho_w}{\rho_b}\right)^{-0.1877} \cdot \left(\frac{\mu_w}{\mu_b}\right)^{-0.3831} \tag{14}$$

Here, the applicable conditions for Eq. (13) are: *Re* must be in the range from 25,000 to 60,000 and *Pr* from 0.73 to 0.79, and for Eq. (14), the applicable *Re* ranges from 25,000 to 60,000. Both relations show reliable predictive accuracy of the CO_2-propane mixture in the semi-circular straight-channel under uniform heat flux heating conditions.

Figure 19 shows the deviation distribution between the predicted values from the fitted correlations and the numerical simulation results. Compared to the other correlations, the newly proposed correlations exhibit smaller prediction deviations and more concentrated distributions. Within the operating range of $P_{c,out}$ = 8.5-18.5 MPa, $T_{c,in}$ = 600-675 K, Re_c = 25,000-60,000, and α = 0.05-0.30, the new correlation predicts the Nu_c and f_c for the CO_2-propane mixture with a deviation less than ±3%.

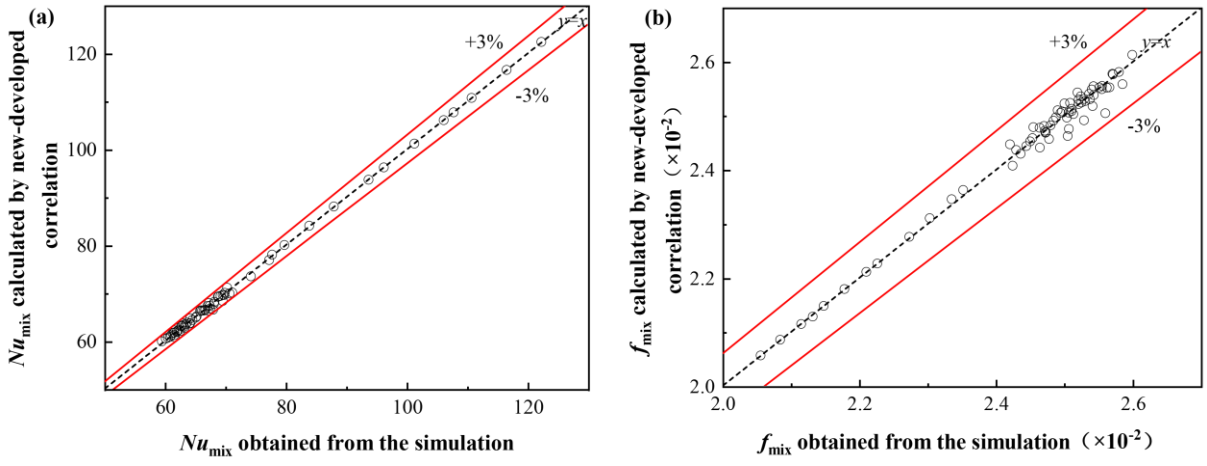

Figure 19. Comparison of CO_2-propane: (a) *Nu*, and (b) *f* between the simulation results and calculated values using the new-developed correlations. The horizontal axis denotes *Nu* and *f* from the simulation results, and the vertical axis from the new-developed correlations.

In summary, for the CO_2-propane mixtures in cold channel, it is recommended to use the new correlation proposed in this study, which has been modified for the mixture. Within the operating range of $P_{c,out}$ = 8.5-18.5 MPa, $T_{c,in}$ = 600-675 K, Re_c = 25,000-60,000, and α = 0.05-0.30, the new correlations predict the *Nu* and *f* for the CO_2-propane with a deviation within ±3%, which demonstrates high accuracy. These correlations are applicable for predicting CO_2-propane mixtures in supercritical state with propane mole fractions ranging from 0.05 to 0.30 in the straight-channel PCHE.

5. Conclusions

The thermodynamic and thermal performance of lead-cooled fast reactors coupled with supercritical CO_2 Brayton power-cycle systems can be further improved by using CO_2-based mixtures, however, the heat transfer and flow characteristics of LBE and CO_2-based mixtures

in various heat exchanger designs remain largely unexplored, and the predictive power of *Nu* and *f* correlations for use in the practical design of relevant systems are unknown. In this study, numerical simulations were conducted to explore the flow and heat transfer characteristics of LBE and CO_2-based mixtures in PCHEs. A range of flows of three different mixtures (CO_2-propane, CO_2-krypton, and CO_2-xenon) were simulated and the results compared, with a focus on LBE and CO_2-propane mixtures under varied operating conditions.

Compared with pure CO_2, CO_2-propane mixture improves the overall heat transfer performance of the PCHE when coupled with LBE, with *U* increasing by up to 40% under the same operating conditions. However, its influence on pressure drop is side-dependent, with an increase on the hot side and a decrease on the cold side. In contrast, the addition of krypton or xenon reduces the cold-side pressure drop but weakens the heat transfer performance compared with the CO_2-propane mixture.

The impact of key parameters (v_{in}, $\dot{m}_{in}$, T_{in}, and P_{out}) on heat transfer was investigated. Increasing the LBE velocity can improve *U* and increasing the mixture mass flow rate improves this by 52% at the same mole fraction of propane. Higher inlet temperatures enhance heat transfer but with limited improvement, while increased system pressure improves mixture heat transfer and has minimal effect on the LBE side.

New *Nu* and *f* correlations for CO_2-propane flows in cold channels with propane mole fractions between 0.05 and 0.30 are proposed, which show good applicability for engineering applications with *Re* ranging from 25,000 to 60,000, with prediction errors within ±3%.

In future work, it is necessary to conduct further investigations into the heat transfer performance using CO_2-based mixtures over a broader range of conditions.

Acknowledgements

The authors gratefully acknowledge the Natural Science Foundation of Shandong Province (no. ZR2024QE199 & no. ZR2025MS819), the "Young Scholar Innovation Team Project" of Higher Education Institutions in Shandong Province (no. 2023KJ002), and the "Taishan Scholar (Young Expert)" program of Shandong Province (no. tsqn202507026). Data supporting this publication can be obtained on request from cep-lab@imperial.ac.uk. For the purpose of Open Access, the authors have applied a CC BY public copyright license to any Author Accepted Manuscript version arising from this submission.

References

[1] Wang T, Wu Z, Xiong W, et al. The impact of uranium resource constraints on China's nuclear power development. *Energies* 2025; 18:1507. https://doi.org/10.3390/en18061507.

[2] He M, Kang H, Lu S, et al. Challenges and solutions to the application of lead-bismuth eutectic alloy coolant. *Rare Metal Mat. Eng.* 2023; 52:3661-72. https://doi.org/10.12442/j.issn.1002-185X.20220753.

[3] Abram T, Ion S. Generation-IV nuclear power: a review of the state of the science. *Energy Policy* 2008; 36:4323-30. https://doi.org/10.1016/j.enpol.2008.09.059.

[4] Wu P, Ma Y, Gao C, et al. A review of research and development of supercritical carbon dioxide Brayton cycle technology in nuclear engineering applications. *Nucl. Eng. Des.* 2020; 368:110767. https://doi.org/10.1016/j.nucengdes.2020.110767.

[5] Liu Y, Wang Y, Huang D. Supercritical CO_2 Brayton cycle: a state-of-the-art review. *Energy* 2019; 189:115900. https://doi.org/10.1016/j.energy.2019.115900.

[6] Song J, Li X, Wang K, et al. Parametric optimisation of a combined supercritical CO_2 (S-CO_2) cycle and organic Rankine cycle (ORC) system for internal combustion engine (ICE) waste-heat recovery. *Energy Conv. Manag.* 2020; 218:112999. https://doi.org/10.1016/j.enconman.2020.112999.

[7] Song J, Li X, Ren X, et al. Thermodynamic and economic investigations of transcritical CO_2-cycle systems with integrated radial-inflow turbine performance predictions. *Appl. Therm. Eng.* 2020; 165:114604. https://doi.org/10.1016/j.applthermaleng.2019.114604.

[8] You M, Zhang F, Liao G, et al. Improvement design and performance assessment of two supercritical carbon dioxide power cycles for waste heat recovery. *Therm. Sci. Eng. Prog.* 2023; 45:102122. https://doi.org/10.1016/j.tsep.2023.102122.

[9] Fan G, Song J, Zhang J, et al. Thermo-economic assessment and systematic comparison of combined supercritical CO_2 and organic Rankine cycle (SCO_2-ORC) systems for solar power tower plants. *Appl. Therm. Eng.* 2024; 236:121715. https://doi.org/10.1016/j.applthermaleng.2023.121715.

[10] Heller L, Glos S, Buck R. Cost benefit analysis of supercritical CO_2 cycles in next-generation solar thermal power plants. *Renew. Energy* 2026; 256:123613. https://doi.org/10.1016/j.renene.2025.123613.

[11] Lu Q, Zhao J, Fang S, et al. Investigation of thermodynamics of the supercritical CO_2 Brayton cycle used in solar power at off-design conditions. *Sustain. Energy Technol. Assess.* 2022; 52:102361. https://doi.org/10.1016/j.seta.2022.102361.

[12] Song J, Loo P, Teo J, et al. Thermo-economic optimization of organic Rankine cycle (ORC) systems for geothermal Power Generation: A comparative study of system configurations. *Front. Energy Res.* 2020; 8:6. https://doi.org/10.3389/fenrg.2020.00006.

[13] Ruiz-Casanova E, Rubio-Maya C, Pacheco-Ibarra JJ, et al. A techno-economic assessment of sCO_2 Brayton cycles for low-grade geothermal reservoirs. *Geothermics* 2023; 113:102775. https://doi.org/10.1016/j.geothermics.2023.102775.

[14] Song J, Wang Y, Wang K, et al. Combined supercritical CO_2 (SCO_2) cycle and organic Rankine cycle (ORC) system for hybrid solar and geothermal power generation: Thermoeconomic assessment of various configurations. *Renew. Energy* 2021; 174:1020-35. https://doi.org/10.1016/j.renene.2021.04.124.

[15] Ahmed MdR, Rokanuzzaman Md, Aziz MdA, et al. Thermo-economic assessment of hybrid solar-driven supercritical CO_2 cycle for multi-generation system. *Energy Conv. Manag.-X* 2025; 28:101290. https://doi.org/10.1016/j.ecmx.2025.101290.

[16] Zhao Y, Song J, Liu M, et al. Thermo-economic assessments of pumped-thermal electricity storage systems employing sensible heat storage materials. *Renew. Energy* 2022; 186:431-56. https://doi.org/10.1016/j.renene.2022.01.017.

[17] Tian R, Xiao X, Wei M, et al. Performance analysis of a carnot battery system coupled $Ca(OH)_2$/CaO thermochemical heat storage and coal-fired power plant. *Renew. Energy* 2026; 256:123922. https://doi.org/10.1016/j.renene.2025.123922.

[18] Ren Z, Zhao CR, Jiang PX, et al. Investigation on local convection heat transfer of supercritical CO_2 during cooling in horizontal semicircular channels of printed circuit heat

675 exchanger. *Appl. Therm. Eng.* 2019; 157:113697.
676 https://doi.org/10.1016/j.applthermaleng.2019.04.107.

677 [19] Li MJ, Zhu HH, Guo JQ, et al. The development technology and applications of
678 supercritical CO_2 power cycle in nuclear energy, solar energy and other energy industries. *Appl.*
679 *Therm. Eng.* 2017; 126:255-75. https://doi.org/10.1016/j.applthermaleng.2017.07.173.

680 [20] Dostal V, Hejzlar P, Driscoll MJ. High-performance supercritical carbon dioxide cycle for
681 next-generation nuclear reactors. *Nucl. Technol.* 2006; 154:265-82.
682 https://doi.org/10.13182/NT154-265.

683 [21] Li MJ, Xu JL, Cao F, et al. The investigation of thermo-economic performance and
684 conceptual design for the miniaturized lead-cooled fast reactor composing supercritical CO_2
685 power cycle. *Energy* 2019; 173:174-95. https://doi.org/10.1016/j.energy.2019.01.135.

686 [22] Zhou Y, Zhang Y, Li H, et al. Off-design operation of supercritical CO_2 Brayton cycle
687 arranged with single and multiple turbomachinery shafts for lead-cooled fast reactor. *Energy*
688 2024; 299:131384. https://doi.org/10.1016/j.energy.2024.131384.

689 [23] Song KN, Hong SD, Ro DS. Measurement of weld mechanical properties of SUS316L
690 plate using an instrumented indentation technique. *J. Weld. Join.* 2013; 31:37-42.
691 https://doi.org/10.5781/KWJS.2013.31.2.37.

692 [24] Ma Y, Liu D, Wang J, et al. Thermal-hydraulic performance and optimization of printed
693 circuit heat exchangers for supercritical fluids: a review. *Renew. Sust. Energy Rev.* 2025;
694 208:115051. https://doi.org/10.1016/j.rser.2024.115051.

695 [25] Xu H, Duan C, Ding H, et al. The optimization for the straight-channel PCHE size for
696 supercritical CO_2 Brayton cycle. *Nucl. Eng. Technol.* 2021; 53:1786-95.
697 https://doi.org/10.1016/j.net.2020.12.002.

698 [26] Yoon SH, No HC, Kang GB. Assessment of straight, zigzag, S-shape, and airfoil PCHEs
699 for intermediate heat exchangers of HTGRs and SFRs. *Nucl. Eng. Des.* 2014; 270:334-43.
700 https://doi.org/10.1016/j.nucengdes.2014.01.006.

701 [27] Huang C, Cai W, Wang Y, et al. Review on the characteristics of flow and heat transfer in
702 printed circuit heat exchangers. *Appl. Therm. Eng.* 2019; 153:190-205.

https://doi.org/10.1016/j.applthermaleng.2019.02.131.

[28] Zhang H, Wang J, Pan J, et al. Investigations on cooling heat transfer of CO_2-based mixtures in a novel airfoil fin mini-channel at supercritical pressure. *Appl. Therm. Eng.* 2024; 255:124010. https://doi.org/10.1016/j.applthermaleng.2024.124010.

[29] Jeong WS, Lee JI, Jeong YH. Potential improvements of supercritical recompression CO_2 Brayton cycle by mixing other gases for power conversion system of a SFR. *Nucl. Eng. Des.* 2011; 241:2128-37. https://doi.org/10.1016/j.nucengdes.2011.03.043.

[30] Di Marcoberardino G, Invernizzi CM, Iora P, et al. Experimental and analytical procedure for the characterization of innovative working fluids for power plants applications. *Appl. Therm. Eng.* 2020; 178. https://doi.org/10.1016/j.applthermaleng.2020.115513.

[31] Invernizzi CM, van der Stelt T. Supercritical and real gas Brayton cycles operating with mixtures of carbon dioxide and hydrocarbons. *Proc. Inst. Mech. Eng. Part A-J. Power Energy* 2012; 226:682-93. https://doi.org/10.1177/0957650912444689.

[32] Guo JQ, Li MJ, Xu JL, et al. Thermodynamic performance analysis of different supercritical Brayton cycles using CO_2-based binary mixtures in the molten salt solar power tower systems. *Energy* 2019; 173:785-98. https://doi.org/10.1016/j.energy.2019.02.008.

[33] Liu X, Xu Z, Xie Y, et al. CO_2-based mixture working fluids used for the dry-cooling supercritical Brayton cycle: thermodynamic evaluation. *Appl. Therm. Eng.* 2019;162:114226. https://doi.org/10.1016/j.applthermaleng.2019.114226.

[34] Ma YN, Hu P, Jia CQ, et al. Thermo-economic analysis and multi-objective optimization of supercritical Brayton cycles with CO_2-based mixtures. *Appl. Therm. Eng.* 2023; 219:119492. https://doi.org/10.1016/j.applthermaleng.2022.119492.

[35] M Guo J, Song J, Zhao Y, et al. Thermo-hydraulic performance of heated vertical flows of supercritical CO_2. *Int. J. Heat Mass Transf.* 2022; 199:123437. https://doi.org/10.1016/j.ijheatmasstransfer.2022.123437.

[36] Guo J, Song J, Han Z, et al. Investigation of the thermohydraulic characteristics of vertical supercritical CO_2 flows at cooling conditions. *Energy* 2022; 256:124628. https://doi.org/10.1016/j.energy.2022.124628.

[37] Sun F, Xie G, Song J, et al. Thermal characteristics of in-tube upward supercritical CO_2 flows and a new heat transfer prediction model based on artificial neural networks (ANN). *Appl. Therm. Eng.* 2021; 194:117067. https://doi.org/10.1016/j.applthermaleng.2021.117067.

[38] Liu H, Zhang Z, Yang S, et al. Numerical investigation on flow and heat transfer characteristics of a PCHE with liquid lead-bismuth eutectic and sCO_2 as working fluids. *Ann. Nucl. Energy* 2024; 200:110367. https://doi.org/10.1016/j.anucene.2024.110367.

[39] Zhou T, Yao Y, Jiang Y, et al. Study on the Coupled Heat Transfer Characteristics of Liquid Lead-Bismuth Eutectic and Supercritical CO_2. *In: Proceedings of the 23rd Pacific Basin Nuclear Conference, Volume 3, vol. 285;* 2023, p. 780-91. https://doi.org/10.1007/978-981-19-8899-8_75.

[40] Xu P, Zhou T, Fu Z, et al. Heat transfer performance of liquid lead-bismuth eutectic and supercritical carbon dioxide in double D-type straight channel. *Appl. Therm. Eng.* 2023; 219:119484. https://doi.org/10.1016/j.applthermaleng.2022.119484.

[41] Fu X, Cai S, Qiu G, et al. Optimization study on PCHE channels for lead-bismuth eutectic and supercritical carbon dioxide coupled flow and heat transfer. *Nucl. Eng. Des.* 2025; 435:113942. https://doi.org/10.1016/j.nucengdes.2025.113942.

[42] Kim IH, No HC. Thermal-hydraulic physical models for a Printed Circuit Heat Exchanger covering He, He-CO_2 mixture, and water fluids using experimental data and CFD. *Exp. Therm. Fluid Sci.* 2013; 48:213-21. https://doi.org/10.1016/j.expthermflusci.2013.03.003.

[43] Yin D, Zhou Y, Guo X, et al. Numerical analysis of wavy PCHEs in supercritical CO_2/propane mixture Brayton cycle. *Appl. Therm. Eng.* 2023; 235:121346. https://doi.org/10.1016/j.applthermaleng.2023.121346.

[44] Yin D, Zhou Y, Guo X. Study on heat transfer characteristics of supercritical CO_2/propane mixtures in vertical tube. *Ann. Nucl. Energy* 2024; 196:110223. https://doi.org/10.1016/j.anucene.2023.110223.

[45] Yan C, Shi J, Zhang S, et al. Investigation on heat transfer of supercritical CO_2/Xe mixture crossing pseudo-critical temperature cooled in a horizontal circular tube. *Appl. Therm. Eng.* 2024; 257:124245. https://doi.org/10.1016/j.applthermaleng.2024.124245.

[46] Ma Y-N, Hu P. Analysis of the Thermal-Hydraulic Characteristics of Supercritical CO_2/Kr Mixtures in the Straight-Channel Printed Circuit Heat Exchanger. *Energy Power and*

Automation Engineering, Singapore: Springer Nature; 2024, p. 3-13. https://doi.org/10.1007/978-981-99-8878-5_1.

[47] Zhou Y, Yin D, Guo X. Flow and heat transfer performance of molten salt and CO_2-based mixtures in printed circuit heat exchangers. *Appl. Therm. Eng.* 2023; 224:120104. https://doi.org/10.1016/j.applthermaleng.2023.120104.

[48] Zhou Y, Yin D, Guo X, et al. Numerical modeling and transient analysis of printed circuit heat exchangers in the supercritical CO_2/propane mixture Brayton cycle. *Int. J. Heat Mass Transf.* 2024; 231:125896. https://doi.org/10.1016/j.ijheatmasstransfer.2024.125896.

[49] Sung J, Lee JY. Effect of tangled channels on the heat transfer in a printed circuit heat exchanger. *Int. J. Heat Mass Transf.* 2017; 115:647-56. https://doi.org/10.1016/j.ijheatmasstransfer.2017.07.091.

[50] Wen Z, Lv Y, Li Q, et al. Numerical study on heat transfer behavior of wavy channel supercritical CO_2 printed circuit heat exchangers with different amplitude and wavelength parameters. *Int. J. Heat Mass Transf.* 2020; 147:118922. https://doi.org/10.1016/j.ijheatmasstransfer.2019.118922.

[51] Liu H, Zhang Z, Du H, et al. Numerical study on the heat transfer characteristics of a microchannel heat exchanger with liquid lead–bismuth eutectic and supercritical CO_2 as working fluids. *Ann. Nucl. Energy* 2023; 192:109990. https://doi.org/10.1016/j.anucene.2023.109990.

[52] Fazio C, Sobolev VP, Aerts A, et al. Handbook on Lead-bismuth Eutectic Alloy and Lead Properties, Materials Compatibility, Thermal-hydraulics and Technologies - 2015 Edition 2015. https://publikationen.bibliothek.kit.edu/1000073814.

[53] Johnson HA, Hartnett JP, Clabaugh WJ. Heat Transfer to Molten Lead-Bismuth Eutectic in Turbulent Pipe Flow. Trans. Am. Soc. Mech. Eng. 1953; 75:1191-8. https://doi.org/10.1115/1.4015579.

[54] Liu H, Zhang Z, Du H, et al. Numerical study on the heat transfer characteristics of a liquid lead-bismuth eutectic in a D-type channel. Front. Energy Res. 2022; 10. https://doi.org/10.3389/fenrg.2022.1041900.

[55] Cheng X, Tak N. Investigation on turbulent heat transfer to lead-bismuth eutectic flows in circular tubes for nuclear applications. *Nucl. Eng. Des.* 2006; 236:385-93. https://doi.org/10.1016/j.nucengdes.2005.09.006.

[56] ANSYS Fluent Theory Guide, ANSYS Inc., Canonsburg, 2024.

[57] Meshram A, Jaiswal AK, Khivsara SD, et al. Modeling and analysis of a printed circuit heat exchanger for supercritical CO_2 power cycle applications. *Appl. Therm. Eng.* 2016; 109:861-70. https://doi.org/10.1016/j.applthermaleng.2016.05.033.

[58] Han Z, Guo J, Chen J, et al. Experimental and numerical investigations on thermal-hydraulic characteristics of supercritical CO_2 flows in printed circuit heat exchangers. *Int. J. Therm. Sci.* 2023; 194:108573. https://doi.org/10.1016/j.ijthermalsci.2023.108573.

[59] Ma N, Bu Z, Fu Y, et al. An operation strategy and off-design performance for supercritical brayton cycle using CO_2-propane mixture in a direct-heated solar power tower plant. *Energy* 2023; 278:127882. https://doi.org/10.1016/j.energy.2023.127882.

[60] Skupinski E, Tortel J, Vautrey L. Determination des coefficients de convection d'un alliage sodium-potassium dans un tube circulaire. *Int. J. Heat Mass Transf*. 1965; 8:937-51. https://doi.org/10.1016/0017-9310(65)90077-3.

[61] Kirillov P, Ushakov PA. Heat transfer to liquid metals: specific features, methods of investigation, and main relationships. *Therm. Eng.* 2001; 48:50-9. https://api.semanticscholar.org/CorpusID:99329821.

[62] Sleicher CA, Awad AS, Notter RH. Temperature and eddy diffusivity profiles in NaK. *Int. J. Heat Mass Transf.* 1973; 16:1565-75. https://doi.org/10.1016/0017-9310(73)90184-1.

[63] Theologou K, Mertz R, Laurien E, et al. Experimental investigations on heat transfer of CO_2 under supercritical pressure in heated horizontal pipes. *Energy* 2022; 254:124171. https://doi.org/10.1016/j.energy.2022.124171.

[64] Filonenko G.K. Hydraulic resistance in pipes. *Teploenergetika* 1954; 1:40-4. https://www.sid.ir/paper/536819/en.

[65] Chen SK, Todreas NE, Nguyen NT. Evaluation of existing correlations for the prediction of pressure drop in wire-wrapped hexagonal array pin bundles. *Nucl. Eng. Des.* 2014; 267:109-31. https://doi.org/10.1016/j.nucengdes.2013.12.003.